Journal of Statistical Physics, Vol. 104, Nos. 1/2, 2001

Scaling, Optimality, and Landscape Evolution

Jayanth R. Banavar,[1] Francesca Colaiori,[2] Alessandro Flammini,[3] Amos Maritan,[3, 4] and Andrea Rinaldo[5]

Received August 8, 2000; revised February 19, 2001

A nonlinear model is studied which describes the evolution of a landscape under the effects of erosion and regeneration by geologic uplift by mean of a simple differential equation. The equation, already in wide use among geomorphologists and in that context obtained phenomenologically, is here derived by reparametrization invariance arguments and exactly solved in dimension $d = 1$. Results of numerical simulations in $d = 2$ show that the model is able to reproduce the critical scaling characterizing landscapes associated with natural river basins. We show that configurations minimizing the rate of energy dissipation (optimal channel networks) are stationary solutions of the equation describing the landscape evolution. Numerical simulations show that a careful annealing of the equation in the presence of additive noise leads to configurations very close to the global minimum of the dissipated energy, characterized by mean field exponents. We further show that if one considers generalized river network configurations in which splitting of the flow (i.e., braiding) and loops are allowed, the minimization of the dissipated energy results in spanning loopless configurations, under the constraints imposed by the continuity equations. This is stated in the form of a general theorem applicable to generic networks, suggesting that other branching structures occurring in nature may possibly arise as optimal structures minimizing a cost function.

KEY WORDS: Rivers; scaling; landscape evolution; optimal transportation networks.

[1] Department of Physics and Center for Materials Physics, 104 Davey Laboratory, The Pennsylvania State University, University Park, Pennsylvania 16802.
[2] Department of Physics and Astronomy, University of Manchester, M13-9PL, Manchester, United Kingdom.
[3] International School for Advanced Studies (S.I.S.S.A.), Via Beirut 2-4, 34014 Trieste, Italy and INFM.
[4] The Abdus Salam International Center for Theoretical Physics, Trieste, Italy.
[5] Dipartimento IMAGE, Universita' di Padova, V. Loredan 20, 35131 Padova, Italy.

0022-4715/01/0700-0001$19.50/0

1. INTRODUCTION

Branching river networks are one of the most common examples of fractal patterns spontaneously produced in nature. The drainage network in a river basin has a tree-like structure which provides an efficient means of transportation and shows clear evidence of fractal behavior, characterized by the absence of a well defined length scale. An account of previous research with an extensive list of references can be found in ref. 1.

Numerous efforts to model the production zone of a river (where the water is collected from relatively uniform spatial patterns of rainfall injection during landscape-forming events. Thus leading flow rates (fluxes) may be assumed as proportional to total contributing areas[1]) have primarily focused on reproducing the statistical characteristics of the drainage network. Less attention has been paid to the temporal behavior and to the evolution of the soil height profile. Recently, this issue has been addressed by many authors.[2–6] Here we discuss a nonlinear model which describes the evolution of a landscape under the effects of erosion by means of a simple differential equation. A brief summary of some of the results of this paper has appeared in ref. 6. This model simulates the evolution of a featureless surface to a morphologically realistic landscape, due to effects of erosion.

Data on the landscape of a basin are obtained in the form of *Digital Elevation Map*s (DEM)[7–9] consisting of discretized elevation fields remotely acquired and objectively manipulated. The discretization units are called *pixels* and are boxes of about $10 \times 10\ m^2$ in a square grid. The drainage network is determined from a DEM assigning to each pixel a drainage direction. Assuming that water flows downhill through steepest descent, an assumption deemed reasonable at the scales of interest, drainage directions go from each pixel to the nearest neighbor with the lowest height. Multiple flow directions occur in topographically convex sites,[10] or in braided patterns.[1] The former arise where hillslope processes dominate whereas here we address scales where fluvial erosion processes are the chief landforming processes, and the latter are excluded because they seldom occur in the production zone. This occurrence of looping structures and multiple flow directions will, however, be further addressed in the last part of this paper.

To each pixel i one can associate a variable that gives the number of pixels draining through i. This quantity represents the total drainage area (*total contributing, or accumulated area*) a_i at the point i, expressed in pixel units, and, in the case of uniform rainfall, provides a measure of the flow at that point. The *upstream length* l_i at the point i is defined as the distance from the farthest source draining into i, measured along the stream (see Fig. 1).

In a first approximation, channels may be defined as being made of those pixels with total drainage area greater than a support area threshold, even though it has been argued[10] that the support area alone may not be sufficient to determine channel initiation.

Observations have lead to a lot of empirical relations between quantities characterizing rivers morphology. *Hack's law* (1957),[11, 12] relates the upstream length at a given position to the accumulated area a at that position: $l = ka^h$ with $k \simeq 1.4$ and $h \simeq 0.6$ (see below for a precise formulation of this scaling law).

This relation is true both for sub-basins of the same basin and for the whole basin of different rivers with approximately the same values for k and h. The departure of the observed value of h from the naive value $\frac{1}{2}$ lead to the first conjectures about the fractality of rivers.[13] Another empirical relation (*slope-discharge*) is between the accumulated area, a, in a point and the gradient of the height of the landscape at that point: $|\vec{\nabla} z| \propto a^{\gamma-1}$ with a numerical value of γ around 0.5. The distributions of accumulated areas a_i and upstream lengths l_i are characterized by power law distributions (with the expected finite size corrections) with exponents τ and ψ respectively, in the ranges $1.40-1.46$ and $1.67-1.85$.[12]

Recently, a lot of effort has been expended in order to define static models able to reproduce these statistical characteristics of real rivers (for a review see ref. 1).

Real drainage basins are not static but usually evolve on extremely long time scales. Nevertheless, some statistical properties seem to be preserved during the evolution. This follows from the fact that some quantities characterizing river basin morphology are almost the same for all rivers, irrespective of their "age."

Our aim is to find the simplest model that simulates the dynamical evolution of morphologically realistic landscapes and that preserves certain features during evolution. The equation we propose to describe the evolution of the landscape is

$$\dot{Z}(t, \underline{x}) = -\alpha J(t, \underline{x}) |\vec{\nabla} Z(t, \underline{x})|^2 + D\nabla^2 Z(t, \underline{x}) + c, \tag{1}$$

where Z denotes the elevation at the point $\underline{x} = (x, y)$ of the substrate plane and J is the modulus of the water flux at that point at time t. The first term is an erosional term proportional to the flux, the second is a diffusive term, and the third is a constant term modeling what geomorphologists call the *uplift*. The existence of an uplift originating in tectonic forces is a well known fact in geomorphology:[10, 14] a landscape represents the instantaneous equilibrium of two concurrently active processes, uplift (endogenic) and degradation (exogenic). A stationary state results from the exact balance of these two agents.

A simple argument leading to an equation of the form (1) is the following: the evolution of a landscape has to be of the form $\dot{Z} = F(\vec{\nabla}Z, \nabla^2 Z, ..., J)$, where an explicit dependence on Z is excluded because that would break translational invariance, and the dependence on $\vec{J}$ (a two dimensional vector) is simply through $J = |\vec{J}|$ because $\vec{J}$ is parallel to $\vec{\nabla}Z$. In the small gradient expansion

$$\dot{Z} = A + \vec{B} \cdot \vec{\nabla}Z + C(\vec{\nabla}Z)^2 + \cdots. \tag{2}$$

On observing that, in order to ensure rotational invariance, $\vec{B} \equiv 0$, one recovers an equation of the form (1). In the next section Eq. (1) will be derived by reparametrization invariance.[6, 15, 16]

The constant term in Eq. (1) can be eliminated by simply replacing $Z(t, \underline{x})$ with $z(t, \underline{x}) = Z(t, \underline{x}) - ct$ in Eq. (1), which is equivalent to a frame of reference in which the system drifts with velocity c. In the new coordinates, Eq. (1) can be rewritten as

$$\dot{z}(t, \underline{x}) = -\alpha J(t, \underline{x}) \, |\vec{\nabla}z(t, \underline{x})|^2 + D\nabla^2 z(t, \underline{x}). \tag{3}$$

Recently this equation has been derived with a similar argument by Somfai and Sander.[18] The diffusive term acts on the surface even at points with zero contributing areas unlike the first term which vanishes when the flux becomes zero. In absence of the diffusive term the presence of maxima on the surface will cause the formation of singularities during the evolution, because points at the top of a hill will never be eroded by the first term (both J and $\vec{\nabla}z$ vanish). The presence of at least an infinitesimal diffusive term is then essential in eliminating these singularities. Equation of type (3) for the study of river networks have been also studied using dynamical renormalization group in ref. 19.

In the discretized version of the model each site (pixel) collects at least an unit area and thus no singularities due to a vanishing contributing area appear even in the absence of the diffusive term. Moreover, the discretization implicitly introduces a diffusive effect because it smoothes z on distances of the order of the lattice length and also prevents the occurence of singularities due to a vanishing $\vec{\nabla}z$ when $D = 0$.

Versions of Eq. (3) and of the more general Eq. (2) in which the presence or the value of the coefficients of different terms are subordinated to the modulus of the slope exceeding a given threshold have also been studied.[20] In this paper, we will focus on the simplified version of Eq. (3) in the discretized lattice form obtained by putting $D = 0$.

In fact, due to the coarse grained scale of the elevation field, the effect of the diffusive term would be negligible because it is not relevant to the large size behavior. Thus, from now on, we will consider the equation

$$\dot{z}(t, \underline{x}) = -\alpha J(t, \underline{x}) \, |\vec{\nabla}z(t, \underline{x})|^2. \tag{4}$$

When it is not explicitly stated otherwise, the flux will be taken to be proportional to the drained area and the terminology fluxes and drained areas will be used interchangeably. This corresponds to the assumption of an uniform rainfall acting on the surface.

It should be noted that geomorphologists employ a different version of Eq. (4) (see ref. 1 and reference therein). In fact, by noting that in general empirical evidence suggests slope-area relationships of the type:

$$|\nabla \bar{z}| \propto a^{-m/n}, \qquad m/n \sim 0.5$$

in many fluvial regimes of interest but sometimes rather different from such reference value, it was empirically concluded that the proper landascape evolution equation should be in the form:

$$\dot{z} = -\alpha a^m |\nabla z|^n$$

possibly complemented by a diffusive term portraying hillslope transport. We see no contradiction with our main tenet, which assumes, in the small gradient approximation, that when fluxes substitute total contributing areas, the proper exponents should be $m = 1$, $n = 2$. More generally $J \propto a^m$ with $m \neq 1.0$, a well known empirical fact in hydrology. It is also interesting to note that empirical slope-area relationships significantly different from the $1/2$ slope indicate, within the validity of our scheme, a hydrological inference which is worth future work.

In spite of its simplicity, this model shows a lot of interesting features. Note that the stationary solutions of Eq. (4) (i.e., $\dot{Z} = 0$) are such that

$$|\vec{\nabla} z| \propto J^{-1/2}. \tag{5}$$

which implies $|\vec{\nabla} z| \propto a^{-1/2}$ if $J \propto a$. This is indeed the previously mentioned *slope-discharge* relation and is a well known empirical fact. (In ref. 5 a similar relation $|\vec{\nabla} z| \propto J^{\gamma - 1}$ has been proposed with $\gamma \neq 1/2$).

Numerical simulations of the erosion equation (to be discussed later) show that the evolution is characterized by two distinct time scales (as was noted in ref. 5). The soil elevations are lowered in a nonuniform way by erosion, causing variations in the drainage directions during the evolution. In a lattice model, at any given time, one may represent the drainage directions at all sites by means of a two dimensional map. After a first characteristic time, the *freezing time*, the spanning graph determining the drainage directions in the basin does no longer changes. Erosion keeps acting on the landscape and changes the soil height, but preserves the drainage structure. The second characteristic time, which is much longer, is the *relaxation time* at which the profile reaches its stable shape.

Because many of the measured quantities, such as the distributions of drained areas and mainstream lengths, depend only on the two dimensional map, the existence of a freezing time much smaller than the relaxation time may provide an explanation for the fact that several statistical properties are found to be almost the same for many rivers, irrespective of their age.

This paper is organized as follows: in the next section we show how Eq. (4) can be obtained as a low order gradient expansion of an equation derived by reparametrization invariance arguments.[15, 16] In the third section we solve the equation exactly in $d = 1$ and show that it is equivalent to the Burgers' equation[21] without viscosity. The solution in one dimension not only yields many of the qualitative features of the two dimensional case, but can also be interpreted as the evolution along the mainstream in the physical case ($d = 2$), as long as one properly takes into account the area collected by each point of this stream. The $d = 1$ case turns out also to be useful in order to clarify the role of boundary conditions. In Section 4 we briefly review the finite size scaling ansatz proposed in ref. 22 describing the critical behavior exhibited by river network models, and the scaling laws relating the critical exponents.[23, 24] The results of numerical studies in $d = 2$ are reported in Section 5. The simulations have been performed using a novel algorithm that converges very quickly to stationary solutions and allows to get very good statistics. The critical behavior of the stationary solutions is analyzed in detail in the context of the finite size scaling ansatz, showing perfect consistency with previously proposed scaling relations and reliable quantitative agreement with observational data. Specifically, we study the distributions of accumulated areas and upstream lengths, the profile along the mainstream, and the bifurcation and length ratios.

In Section 6 we briefly review the static model of river networks known as the *Optimal Channel Network* (OCN).[25, 26] The OCN model is based on the ansatz that configurations occurring in nature are those that minimize a functional describing the dissipated energy and on the derivation of an explicit form for such a functional. We prove that optimal networks are strictly related to the stationary solutions of the model proposed here. In particular, we prove that to any configuration that minimize the dissipated energy within the framework of some simple dynamical rules[25, 26] corresponds, through the slope discharge relation, to an elevation field that is a stationary solution of Eq. (4). Motivated by this result, we analyze the temporal behavior of the "topological energy" and show that it decreases monotonically during the evolution.

The OCN model has been already analyzed by the authors in previous papers.[23, 24, 27] The scaling behavior of the global minimum has been worked out analytically and it has been found to yield mean field exponents. Interestingly, local minima also exhibit critical behavior but are

characterized by different nontrivial exponents. The readily accessible stationary solutions of our Eq. (4) seem to belong to the same universality class as the local minima of OCN model. Motivated by these considerations, we performed some simulations of Eq. (4) modified by the presence of an additive noise term, in order to reach more stable solutions. This has been achieved by "heating" the system followed by careful annealing with the additive noise term playing the role of the temperature in the annealing procedure. Results of this analysis are given in Section 7. We find a distinct class of stationary solutions whose critical behavior is characterized by a different set of exponents, corresponding to that of the global minimum of the dissipated energy and in accordance with a mean field model.[23, 28, 29] In the same section we analyze the effect of an additive noise term on the slope-discharge relation (5). In Section 8, we present a novel result in the form of a theorem on general networks, showing that loopless structures may arise from the minimization of a cost function. In the context of river networks, the theorem shows that the fact that their structure is loopless need not to be taken as an assumption, but follows from the minimization of the dissipated energy, with the constraint that a continuity equation for the flow is satisfied. The conclusions and outlook are presented in Section 9.

2. EVOLUTION EQUATION FOR RIVER NETWORKS AND REPARAMETRIZATION INVARIANCE

The evolution of a surface under the effect of erosion can be described in general in terms of an equation of the form

$$\partial_t \vec{r}(\underline{s}, t) = \hat{n}(\underline{s}, t)\, \mathscr{F}[\vec{r}(\underline{s}, t), \vec{J}(\vec{r}(\underline{s}, t)), \vec{G}] \tag{6}$$

where $\vec{r}(\underline{s}, t)$ is a three dimensional vector spanning the surface and $\underline{s} = (s_1, s_2)$ varies in parameter space. $\hat{n}(\underline{s}, t)$ is the unit normal to the surface at $\vec{r}(\underline{s}, t)$, $\vec{G}$ is the gravitational field assumed to be constant on the surface, $\vec{J}(\vec{r}(\underline{s}, t))$ is the flux in the point $\vec{r}$ which is directed along the steepest descent direction of the surface, and $\mathscr{F}$ contains a deterministic erosional mechanism. The time derivative of $\vec{r}$ must be parallel to the normal to the surface. Terms parallel to the surface in Eq. (6) would not change the evolution since by a suitable time dependent change of the parametrization they can be readily absorbed.

Based on general considerations, one can guess the form of $\mathscr{F}$. The first is the reparametrization invariance:[15, 16] irrespective of the details driving the evolution, the equation must satisfy the requirement of independence from the choice of the particular parametrization, $\underline{s}$, we are using

to describe the surface. This means that only quantities that are intrinsic can enter the equation.

The second consideration is that in the absence of flux, erosion does not take place, and leads to $\partial_t \vec{r}$ becoming equal to zero. Indicating with J the modulus of the flux, the simplest hypothesis is:

$$\mathscr{F} = -J\tilde{\mathscr{F}} + \mathcal{O}(J^2). \tag{7}$$

$\tilde{\mathscr{F}}$ is a scalar and thus it must depend on $\hat{n}$ and $\vec{G}$ only by their scalar product $\hat{n}\cdot\vec{G}$. Moreover, when $\hat{n} \,||\, \vec{G}$, no erosion ought to take place causing $\tilde{\mathscr{F}}$ to vanish. This suggests:

$$\tilde{\mathscr{F}} = G + \hat{n}\cdot\vec{G} \tag{8}$$

where G denotes the modulus of $\vec{G}$.

Thus, to first order in J

$$\mathscr{F} = J(G + \hat{n}\cdot\vec{G}) \tag{9}$$

Let us now use for $\vec{r}$ the Monge parametrization. In this parametrization, $\underline{x}$ is a two dimensional vector in the "substrate" plane and $z(\underline{x})$ is the height of the surface in the direction z ($||\,\vec{G}$) perpendicular to that plane. This is not the most general parametrization: the presence of overhangs in the surface is in fact excluded, otherwise the function $z(\underline{x})$ would no more be single valued. Nevertheless, it is general enough for our purposes. In this parametrization, the metric tensor has the form $g_{ij} = \delta_{ij} + \partial_i z\, \partial_j z$ with determinant $g = 1 + |\vec{\nabla} z|^2$. The normal versor is

$$\hat{n} = g^{-1/2}\partial_1\vec{r}\times\partial_2\vec{r} = \frac{(-\vec{\nabla}z, 1)}{\sqrt{1+|\vec{\nabla}z|^2}}. \tag{10}$$

In these coordinates, Eq. (6) reads

$$\partial_t \vec{r}(\underline{x}, z(\underline{x}, t)) = \hat{n}(\underline{x}, z(\underline{x}, t))\, \mathscr{F}. \tag{11}$$

Taking on both sides the scalar product with the versor $\hat{n}$ yields

$$\dot{z} = \mathscr{F}\sqrt{1+|\vec{\nabla}z|^2}, \tag{12}$$

where $\dot{z}$ is the time derivative of z at fixed $\underline{x}$. Thus $\dot{z}/\sqrt{1+|\vec{\nabla}z|^2}$ has the meaning of velocity in the direction perpendicular to the surface. Replacing

in Eq. (12) the expression for $\mathscr{F}$ given by Eq. (9) and using $\vec{G} = G(0, 0, -1)$, one obtains

$$\dot{z} = -GJ(\sqrt{1+|\vec{\nabla}z|^2}-1). \tag{13}$$

To lowest order in a gradient expansion, Eq. (4) is recovered.

Before proceeding, a word of caution is needed here. The above expansion in small gradient terms implicitly assumes that the surface has a certain degree of smoothness that, in general, is unlikely to hold at very small length scales. This problem is rather common in many contexts akin to the one presented here (roughening, for example, see ref. 17). Our description ought to hold in a coarse grained picture corresponding to long length scales, while it may breakdown below a cut-off that we estimate from the data to be of the order of tens to a few hundred meters at the most, depending on vegetational, climatic and other environmental factors. In humid climates, the drainage density, a length scale characteristic of where channels begin, i.e., the distance one has to walk on average from any given point before encountering a channel, is of the order of less than 100 meters. It is generally agreed that the channelized portion of the watershed (that we address) dominates the landscape features at larger scales. In addition, diffusion-like processes are generally acknowledged to smoothen the soil height in the overland region outside the channelized landscape.

3. ANALYTIC SOLUTION IN $d = 1$

Equation (4) in $d = 1$ uniquely determines the evolution of a profile $z(t)$ once the boundary and initial conditions have been chosen. We will study the equation on a segment $[0, L]$. The initial profile $z_0(x)$ and the elevation in L at any time are enough to determine uniquely the solution. In what follows, in particular, we will consider the case in which the point at L moves down with constant velocity v. We will show that this equation has a stationary solution in the sense that, after a certain relaxation time, the profile moves rigidly with a constant velocity v preserving its shape. This is exactly the solution we are interested in, since in the real coordinates $Z(x, t) = z(x, t) + ct$, Z is constant in time if the velocity v is taken to be equal to the uplift speed c, i.e., $v = -c$. For smooth profiles without lakes, $J \propto x$ and then Eq. (4) becomes (after a trivial rescaling of the time in order to absorb the various constants)

$$\partial_t z(x, t) = -x[\partial_x z(x, t)]^2, \qquad x \in [0, L] \tag{14}$$

with boundary conditions

$$\begin{cases} z(x, 0) = z_0(x) \\ \partial_t z(L, t) = -v \qquad (v > 0). \end{cases} \tag{15}$$

With the change of variable $y = \sqrt{x}$ and taking a derivative on both sides with respect to x one gets an equation for $u(y, t) = \partial_y z(y^2, t) = 2\sqrt{x}\, \partial_x z(x, t)\,|_{x=y^2}$:

$$\partial_t u(y, t) = -\tfrac{1}{2} u(y, t)\, \partial_y u(y, t) \tag{16}$$

with boundary conditions

$$\begin{cases} u(y, 0) = u_0(y) = 2y(\partial_x z_0(x))|_{x=y^2} \\ u(\sqrt{L}, t) = -2\sqrt{v}. \end{cases} \tag{17}$$

Note that the boundary conditions (17) give rise to a continuous solution only if $u_0(\sqrt{L}) = -2\sqrt{v}$, i.e., if $\partial_x z_0(x)\,|_L = -\sqrt{v}/\sqrt{L}$.

Equation (16) is a special case of a class of differential equations called *conservation laws*, and related to the problem of shock waves, that have been extensively studied both by physicists and mathematicians. Their solution on $(-\infty, +\infty)$ is well known. We will show that the problem on $[0, L]$ defined by Eq. (16) with the boundary conditions (17) is equivalent to a certain problem on $(-\infty, +\infty)$ and can thus be solved exactly. The general solution of Eq. (16) is implicitly given by (see, for example, ref. 30, Chap. 15)

$$u(y, t) = \hat{u}_0(y - \tfrac{1}{2} t u(y, t)) \tag{18}$$

where $\hat{u}_0$ is a suitable initial condition: $\hat{u}_0$ cannot in fact be any arbitrary function in order for the (18) to be invertible. This condition is satisfied for any $\hat{u}_0$ as long as $\partial_x \hat{u}_0(x) \geqslant \frac{\hat{u}_0(x)}{x}$.

The fact that Eq. (18) provides a solution of Eq. (16) can be checked quite easily by direct substitution. If boundary conditions are postulated in the form

$$\begin{cases} u(y, 0) = u_0(y) \qquad 0 \leqslant y \leqslant A \\ u(A, t) = f(t) \qquad t \geqslant 0 \end{cases} \tag{19}$$

where u_0 and f are specific known functions, then

$$\hat{u}_0(y) = \begin{cases} u_0(y) & 0 \leqslant y \leqslant A \\ f(t(y)) & y \geqslant A \end{cases} \tag{20}$$

where $t(y)$ solves the equation $y = A - \frac{1}{2} t f(t)$. f must be such that Eq. (20) does not contain any ambiguity in the definition of $\hat{u}_0$. In the specific case of Eq. (17) $f = \text{const} = -2\sqrt{v}$, Eq. (20) becomes

$$\hat{u}_0(y) = \begin{cases} 2y(\partial_x z_0(x))|_{x=y^2} & y \in [0, \sqrt{L}) \\ -2\sqrt{v} & y \geqslant \sqrt{L} \end{cases} \tag{21}$$

and thus, through Eq. (18), we have the complete solution for $z(x, t)$, $\forall t > 0$, which, on taking into account Eq. (15), becomes

$$z(x, t) = -\int_x^L \frac{dx'}{2\sqrt{x'}} u(\sqrt{x'}, t) - vt. \tag{22}$$

Such a solution depends on the initial profile z_0 only in the transient regime, while the stationary solution depends only on v and is given by

$$z(x, t) = 2\sqrt{v}(\sqrt{L} - \sqrt{x}) - vt \tag{23}$$

If, for example, the initial condition is simply a straight line with slope $-m$: $z(x, 0) = m(L - x)$, then, from Eqs. (18), (21), and (22) one easily finds

$$z(x, t) = \begin{cases} -\dfrac{mx}{1 - mt} + mL & x < \bar{x}(t) \\ 2\sqrt{v}\,(\sqrt{L} - \sqrt{x}) - vt & x \geqslant \bar{x}(t) \end{cases} \tag{24}$$

where the function $\bar{x}(t)$ is given by

$$\bar{x}(t) = L\left(1 - t\frac{\sqrt{v}}{\sqrt{L}}\right) \tag{25}$$

In this case, there emerges quite clearly a relaxation time for the evolution that could be defined as

$$t_R = \max_{x \in [0, L]} \bar{t}(x) = \frac{\sqrt{L}}{\sqrt{v}}. \tag{26}$$

where $t = \bar{t}(x)$ is the inverse function of $x = \bar{x}(t)$.

In fact, we will show that the discontinuity in $u(x, t)$ does not imply a discontinuity in $z(x, t)$ if the initial condition z_0 is such that $\partial_x z_0(x)|_L \leqslant -\sqrt{v}/\sqrt{L}$. In the example of the straight line, (24) is still a solution, and the function $\bar{x}(t)$ must be determined imposing the continuity of z. Such a function exists for any $m \leqslant \sqrt{v}/\sqrt{L}$ and is given by

$$\bar{x}(t) = \frac{(1-mt)}{m^2}\left(\sqrt{v} - \left(\frac{\sqrt{v} - m\sqrt{L}}{\sqrt{1-mt}}\right)\right)^2 \tag{27}$$

The relaxation time is $t_R = 2\frac{\sqrt{L}}{\sqrt{v}} - \frac{mL}{v}$. If $m = \epsilon\sqrt{\frac{v}{L}}$ with $0 \leqslant \epsilon \leqslant 1$ then $t_R = \sqrt{\frac{L}{v}}(2-\epsilon) \sim \sqrt{\frac{L}{v}}$.

For a generic initial condition $t_R \sim \sqrt{L}$, unless $v = 0$. This can also be easily obtained with the following scaling argument: assuming the scaling of x, z and t with L:

$$x \sim L, \qquad z \sim L^{\alpha}, \qquad t \sim L^{\zeta}, \tag{28}$$

one gets, from Eqs. (14) and (15) that $\alpha - \zeta = 2\alpha - 1 = 0$ and then

$$\alpha = \zeta = 1/2. \tag{29}$$

The solution $z(x, t, L)$ assumes the scaling form

$$z(x, t, L) = \sqrt{L}\, f\left(\frac{x}{L}, \frac{t}{L^{\zeta}}\right), \tag{30}$$

where f is a scaling function given by

$$f(w, k) = -\int_w^1 \frac{ds}{2\sqrt{s}}\, \bar{u}(\sqrt{s}, k) - vk, \tag{31}$$

where $\bar{u}(\sqrt{x/L}, t/\sqrt{L}) = u(\sqrt{x}, t; L)$ and we have used the fact that the function $u(\sqrt{x}, t; L)$ can be expressed in terms of the dimensionless variables $w = x/L$ and $k = t/\sqrt{L}$. This is possible since from Eq. (18) $u \sim L^{\frac{1}{2}-\zeta} = L^0$ (equivalently, from the definition of u, $u \sim L^{\alpha-\frac{1}{2}}$). For $t \geqslant t_R$ the scaling function becomes $f(w, k) = 2\sqrt{v}\,(1 - \sqrt{w}) - vk$. This scaling argument is also useful to analyze the relevance of a possible diffusive term $\partial_x^2 z$ in the equation. Such a term should scale as $L^{\alpha-2} = L^{-3/2}$ and turns out to be irrelevant in the large size limit.

The case $v = 0$ (zero uplift), should be treated separately. When $v = 0$, the boundary condition becomes $z(L, t) = 0, t \geqslant 0$. Then Eq. (21) gives $\hat{u}_0(y) = 0$ for $y \geqslant \sqrt{L}$. In order for the solution to be well defined, one requires $\hat{u}_0(\sqrt{L}) = 0$. Now, let us assume that $y - \frac{1}{2}tu(y, t)$ (the argument of $\hat{u}_0$ in Eq. (18)) can be arbitrarily close to $\sqrt{L}$, for large enough t. This assumption will be verified a posteriori. Then, $\hat{u}_0$ in Eq. (18) can be expanded around $\sqrt{L}$. Let us consider the case $\hat{u}_0'(\sqrt{L}) \neq 0$. To first order,

$$\hat{u}_0(y - \tfrac{1}{2}tu(y, t)) = \hat{u}_0'(\sqrt{L})(y - \tfrac{1}{2}tu(y, t) - \sqrt{L}) \tag{32}$$

where $\hat{u}_0'(\sqrt{L}) \geqslant 0$ being $\hat{u}_0(y) < 0$ for $0 < y < \sqrt{L}$. Equation (32) can be solved for u, yielding

$$u(y, t) = \frac{2(y - \sqrt{L})}{2\hat{u}_0'(\sqrt{L})^{-1} + t}. \tag{33}$$

The hypothesis made above can be easily checked to be true. In terms of z, Eq. (33) gives

$$z(x, t) = \frac{(\sqrt{x} - \sqrt{L})^2}{2\hat{u}_0'(\sqrt{L})^{-1} + t}. \tag{34}$$

for the case $v = 0$ and asymptotic times. This kind of behavior has been found by Sinclair and Ball[5] on assuming that Eq. (4) could be solved by the separation of variables. In this case, the landscape assume a "semi-stationary" shape, in the sense that profiles at different times differ by a factor t^{-1}.

If we now consider the general case in which $\hat{u}_0'(\sqrt{L})$ may also be zero, Eq. (32) must be replaced with

$$\hat{u}_0\left(y - \frac{1}{2}tu(y, t)\right) = \frac{\hat{u}_0^n(\sqrt{L})}{n!}\left(y - \frac{1}{2}tu(y, t) - \sqrt{L}\right)^n \tag{35}$$

where $\hat{u}_0^n(\sqrt{L})$ is the first nonzero derivative of $\hat{u}_0$ in $\sqrt{L}$. Note that $\hat{u}_0^n(\sqrt{L})$ must be negative in order for $u(y, t)$ to be negative which would correspond to a monotonically decreasing profile $z(x, t)$. This equation gives a behavior qualitatively similar to that of Eq. (34).

It is interesting to note that the form of the scaling function in the stationary solution (23) can be obtained from very general considerations and on the scaling assumption, without referring to a specific evolution equation.

For a river of size L let $z(x, L)$ be the height at position x. We impose $z(L, L) = 0$. The height $z(x-y, L)$ with $y > 0$ can be related to the height $z(x, L)$ and to the one of a river of length x at position $x-y$ as follows:

$$z(x-y, L) = z(x, L) + z(x-y, x). \tag{36}$$

In the limit $y \to 0$

$$z(x, L) - yz_1'(x, L) = z(x, L) + z(x, x) - yz_1'(x, x) \tag{37}$$

where $z_1'(x, L) = \frac{\partial z}{\partial x}(x, L)$. From Eq. (37), given that $z(x, x) = 0$, it follows that $\frac{\partial z}{\partial x}(x, L) = z_1'(x, x)$, independent of L. Integrating $\frac{\partial z}{\partial x}(x, L)$ from 0 to L we have

$$z(L, L) - z(x, L) = \int_x^L \frac{\partial z}{\partial s}(s, L)\, ds = \int_x^L z_1'(s, s)\, ds = F(L) - F(x). \tag{38}$$

where F is a primitive of z_1', i.e., $\frac{\partial F}{\partial x}(x) = z_1'(x, x)$. Because $z(L, L) = 0$, we have $z(x, L) = F(x) - F(L)$. This is the general expression that a profile *must* have (up to this point no assumptions have been made).

If we require scaling:

$$z(x, L) = L^{\alpha} f\left(\frac{x}{L}\right) = F(x) - F(L) = F(L)\left(\frac{F(x)}{F(L)} - 1\right), \tag{39}$$

then $F(x) = -Ax^{\alpha}$ implying

$$z(x, L) = AL^{\alpha} f\left(\frac{x}{L}\right), \tag{40}$$

where $A = z(0, L)$ and $f(s) = 1 - s^{\alpha}$. This is exactly what we found in $d = 1$ with $\alpha = 1/2$ and what we will find (see Section 6) for the mainstream in $d = 2$ with the appropriate α.

4. DESCRIPTION OF SCALING LAWS

In order to provide a general setting for further considerations we review some basic concepts about the finite size scaling approach to the statistical characterization of river networks. Such networks are known to exhibit power law behavior typical of fractal structures in the distributions of some quantities characterizing their morphology. Let us define such distributions in the simple case of a lattice model which will be used explicitly in the next sections.

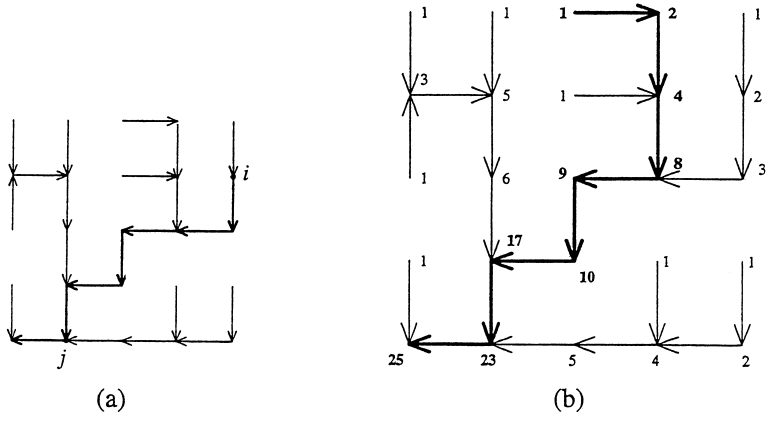

Fig. 1. Example of drainage network. The outlet is the bottom left corner. In (a) the site i is upstream with respect to the site j. The upstream length l_j of site j is 7 in this case. In (b) the numbers correspond to the drained areas (assuming a uniform unit precipitation rate) and the bold line to the mainstream.

A landscape is described by a scalar field of elevation, where drainage directions are identified by steepest descents, i.e., by the direction of the largest local decrease of the elevation field. Excluding the presence of lakes, i.e., assuming that from each point the water does flow to one of the nearest neighbors, a river network can be represented by an oriented spanning graph over a two dimensional lattice of arbitrary size and shape, in which oriented links (one coming out from each site of the lattice) correspond to drainage directions.

To fix the ideas, consider a loopless oriented graph spanning an $L \times L$ square lattice, with outlets on one edge. We will say that a point i is *upstream* with respect to a point j if there exists an oriented path joining the two points from i to j (see Fig. 1). To each site i of the lattice, we associate a local injection r_i, representing the "injection (or critical rainfall) intensity" in the site i.

The flow J_i, can thus be defined as the sum of the injections over all the points upstream of site i, site i included. In the case of constant injection ($r_i \equiv$ constant), the flow in a point i results to be proportional to the area a_i drained in that point and we will use these two quantities interchangeably. In natural basins these drained areas can be investigated through data obtained from digital elevation maps (DEM's).[7–9]

By definition, the variables J_i are related by the following set of equations:

$$J_i = \sum_j w_{i,j} J_j + r_i \,, \tag{41}$$

where $w_{i,j}$ is 1 if site j is a nearest neighbor upstream with respect to site i and 0 otherwise.

Another relevant quantity is the so called upstream length relative to a site, defined operationally as the length of the stream obtained starting from that site and repeatedly moving along the network in the upstream direction towards the nearest-neighbor with biggest area (the one leading to the outlet is excluded, since it is a downstream site), until a source is reached, i.e., a site with no incoming links. If two or more equal areas are encountered, one is randomly selected.

For a given graph on a lattice of given linear size L, we will consider the following two probability distributions originally introduced to describe river basins and experimentally found to scale as power laws: $p(a, L)$, the probability density of drained areas a and $\pi(l, L)$, the probability density of the upstream lengths l. These represent the fraction of sites draining an area a or having an upstream length l respectively. We will also consider the corresponding integrated probability distributions $P(a, L)$, and $\Pi(l, L)$. For such distributions a finite size scaling ansatz has been formulated[22] that seems to provide a simple and natural explanation to well known empirical laws. The finite size scaling ansatz consists in postulating the following form for the distributions:

$$p(a, L) = a^{-\tau} f\left(\frac{a}{a_C}\right), \tag{42}$$

$$\pi(l, L) = l^{-\psi} g\left(\frac{l}{l_C}\right), \tag{43}$$

where $f(x)$ and $g(x)$ are scaling functions accounting for finite size effects and a_C and l_C are the characteristic area and length respectively which depend on L. The functions $f(x)$ and $g(x)$ are assumed to have the following properties: when $x \to \infty$ they go to zero sufficiently fast to ensure normalization; when $x \to 0$ they tend to a constant, to yield simple power law behavior of the probability distributions in the large size limit. This also implies that τ and ψ are bigger than one.

The characteristic area and length are assumed to scale as

$$a_C \sim L^{1+H}, \tag{44}$$

$$l_C \sim L^{d_f}. \tag{45}$$

H is known as the Hurst exponent and satisfies $0 \leqslant H \leqslant 1$. The d_f exponent, characterizing the typical length, has the meaning of the fractal

dimension of a stream (each rivulet going from any site to the outlet is assumed to have the same fractal dimension), and is such that $1 \leqslant d_f \leqslant 1+H$.

$d_f = 1$ corresponds to a straight line, whereas $d_f = 1+H$ corresponds to the situation of virtually one space filling rivulet.

The integrated probability distributions can be written as

$$P(a, L) = a^{1-\tau} F\left(\frac{a}{L^{1+H}} \right), \tag{46}$$

$$\Pi(l, L) = l^{1-\psi} G\left(\frac{l}{L^{d_f}} \right), \tag{47}$$

which follow from (42) and (43) with

$$F(x) = x^{\tau-1} \int_x^{+\infty} dy \; y^{-\tau} f(y), \tag{48}$$

$$G(x) = x^{\psi-1} \int_x^{+\infty} dy \; y^{-\psi} g(y). \tag{49}$$

The four exponents introduced up to now are not independent. In fact they have been shown[22–24, 31] to be related by the following scaling laws:

$$\tau = 2 - \frac{d_f}{1+H}, \tag{50}$$

$$\psi = \frac{1+H}{d_f}. \tag{51}$$

Essentially, the former equation follows from the consideration that the average over all the sites of the accumulated areas and of the distances from the outlet are equal; the latter equation from a consistency requirement for the conditional probability distribution of upstream lengths l given an accumulated area a.

The observed values of τ and ψ are in the ranges 1.40–1.46, 1.67–1.85 respectively.

A well known hydrological law, Hack's law,[11] relates the length of the longest stream l in the drainage region to the drainage area of the basin a:

$$l \sim a^h. \tag{52}$$

The accepted values of h range in the interval $h = 0.56 \pm 0.02$.[32–34] Their definite departure from the Euclidean value 0.5 lead to the first suggestion of the fractal nature of rivers.[13] From Eqs. (44) and (45) it follows that

$$h = \frac{d_f}{1+H}. \tag{53}$$

The scaling relations (50) and (51) can be expressed in a simpler form, observing that both τ and ψ depend on d_f and H only in the combination $d_f/(1+H) = h$, where h is the exponent appearing in Hack's law (52). Thus

$$\tau = 2 - h, \tag{54}$$

$$\psi = \frac{1}{h}. \tag{55}$$

The exponents τ and ψ are thus related by the simple expression:

$$\tau = 2 - \frac{1}{\psi}. \tag{56}$$

Since $1 \leqslant d_f \leqslant 1+H$ and $H \leqslant 1$ it follows that $1/2 \leqslant h \leqslant 1$. This implies that $\tau \leqslant 3/2$. The equality holds only when $H = d_f = 1$ which corresponds to the mean field situation.[23, 24, 28, 29]

5. TWO-DIMENSIONAL RIVER NETWORKS

In this section we report our results on the analysis of Eq. (4) in $d = 2$, corresponding to the physical case. These results come from computer simulations combined with some analytical arguments.

In Section 5.1 we describe an iterative algorithm for the search of stationary solutions of Eq. (4). All data regarding the stationary solutions have been obtained with this method. They are analyzed in detail in Sections 5.2, 5.3, and 5.4.

All simulations described in this section refer to a square lattice with periodic boundary conditions in one direction and open boundary conditions in the other one.

5.1. Description of the Iterative Algorithm

Any stationary solution of Eq. (4) must satisfy

$$\alpha J \, |\vec{\nabla} z|^2 = v, \tag{57}$$

where v is a constant velocity imposed by the boundary conditions, on the lower edge. Thus for a stationary solution, the relation

$$|\vec{\nabla} z| = \sqrt{\frac{v}{\alpha}}\, J^{-\frac{1}{2}} \tag{58}$$

between flux and gradient must hold at any point.

In a discrete version, the landscape is described on specifying a field of elevation $\{z_i\}$ (a measure of the gradient of z is obtained by the biggest drop in elevation at site i). We assume, following the observational data, that there are no lakes or at least that the lakes have been removed by identifying the flow direction for the water from a lake when it overflows. The drainage basin can be reconstructed using the rule of *steepest descent*, i.e., the flux in a point has the direction of the maximum gradient of the elevation field (the direction towards the lowest among all its nearest neighbors). One can thus uniquely associate any landscape (without local height minima corresponding to lakes) with an oriented spanning graph on the lattice, i.e., an oriented loopless graph passing through each point. Now, identifying the flux in a point with the total area drained in that point, one can reconstruct the field of fluxes $\{J_i\}$ corresponding to a given oriented spanning graph. The flux in a site is simply given by the number of sites upstream with respect to that site in the case of uniform rainfall, and is given by Eq. (41) in the more general case. From the fluxes, a new field of elevation can be defined using Eq. (58). The new configuration of the landscape will again not form lakes because each point has at least one nearest neighbor with a biggest flux, which includes the one into which it flows, and therefore from (58) it has at least one nearest neighbor with smaller height.

We can then define a transformation from the set of lake-less configurations on to itself:

$$\{z_i'\} = \mathscr{T}(\{z_i\}) \tag{59}$$

where $\mathscr{T}$ consists in the following chain of transformations:

$$\{z_i\} \xrightarrow{\text{steepest descent}} \begin{matrix}\text{spanning}\\ \text{graph}\end{matrix} \xrightarrow{\text{drained areas}} \{J_i\} \xrightarrow{\text{equation (58)}} \{z_i'\}$$

Any fixed point of Eq. (59) is a stationary solution of Eq. (4).

5.2. Scaling of Drained Areas and Upstream Lengths

We performed simulations on samples of different sizes starting for each size with 100 different initial conditions.

A randomly generated surface is not, in general lake-less. Usually, initial conditions are constructed giving a random surface and then "filling up" the lakes. This procedure proves to be very slow. To further speed up the algorithm, we generated initial conditions from a spanning graph followed by steps 2 and 3 of the algorithm.

The initial spanning graphs were constructed in the following way: we choose a site at random as an origin of a random walk that terminated when it reached a site on the edge containing the outlets. Then another site is randomly selected among the ones not visited by the previous walks and a new random walk is generated till it visits one site on the edge containing the outlets or it intersect the already existent pattern (consisting of the union of the previous random walk(s) *but* the present). If, before this happens the walk intersects itself at some point i, then the older of the two links emerging from i is deleted in order to eliminate the loop. This procedure is repeated until all sites have been incorporated. The distributions (46) and (47) of such spanning graphs has been tested in order to check to which universality class (assumed to be identified by the power laws exponents introduced in Section 4), they belong to. We found $\tau = 1.40 \pm 0.03$ and $\psi = 1.67 \pm 0.03$.

For sizes 32, 64, 128 and 256, starting from configurations generated in this way and iterating the algorithm described in Section 5.1 we got stationary solutions of Eq. (4). The distributions of the resulting drained areas and upstream lengths show power law behavior. The exponents are nearly the same for each configuration and are different from the ones we started from. Averages over the 100 stationary conditions give for the exponents

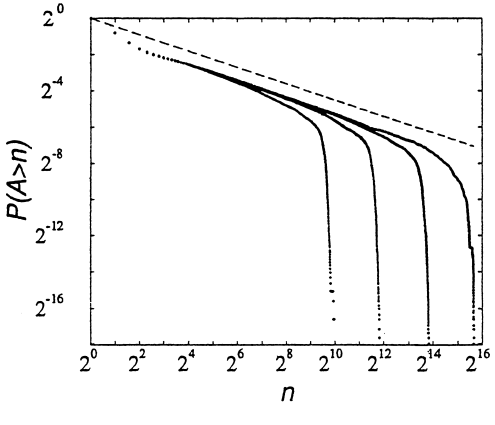

Fig. 2. Integrated probability distribution of accumulated areas averaged over 100 samples on 32×32, 64×64, 128×128 and, 256×256 square lattices. The slope of the dashed line is $\tau - 1 = 0.45$.

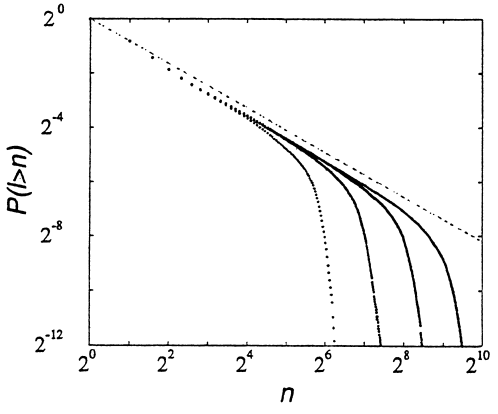

Fig. 3. Integrated probability distribution of mainstream lengths averaged over 100 samples on 32×32, 64×64, 128×128, and 256×256 square lattices. The slope of the dashed line is $\psi - 1 = 0.82$.

$\tau = 1.45 \pm 0.02$ and $\psi = 1.82 \pm 0.02$. Log–log plots of these integrated probability distributions of accumulated areas and upstream lengths are shown in Figs. 2 and 3. Collapse tests have been carried out in order to evaluate the exponents defining the characteristic area and length that yield: $1 + H = 1.98 \pm 0.04$ and $d_f = 1.10 \pm 0.04$. The collapse plots are shown in Figs. 4 and 5. These numerical values are in perfect agreement with the scaling relations in Section 4.

To have a direct measure of the exponent h appearing in Hack's law, we plotted the drained areas along the mainstream with respect to the

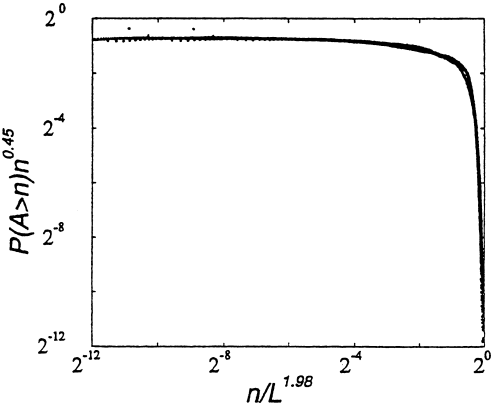

Fig. 4. Collapse plot for the distributions of Fig. 2 obtained with $\tau = 1.45$ and $1 + H = 1.98$.

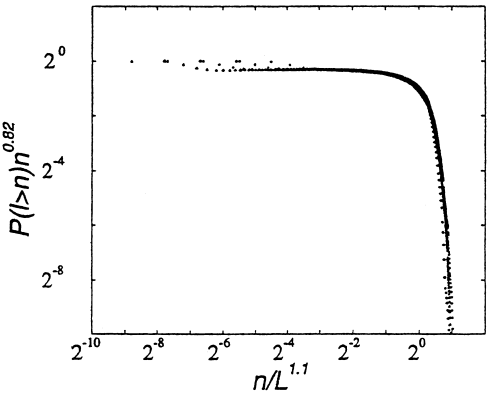

Fig. 5. Collapse plot for the distributions of Fig. 3 obtained with $\psi = 1.82$ and $d_f = 1.1$.

corresponding upstream length (inset in Fig. 7). We found a good power law with an exponent $h = 0.55 \pm 0.02$ in good agreement both with the values of H and d_f and with the value observed in natural basins.

We note that the values of the exponents we found are quite close to "trivial" ones ($d_f = 1, \tau = 3/2$, for example) , so that one might wonder if what we are really seeing are corrections to scaling rather than a genuine non-trivial universality class. To test such an eventuality we tried more complicated fits, but this involved the introduction of additional parameters (in the form of coefficents and exponents). It becomes hard to judge whether such fits are warrented from the data on hand. Our view has been that the most important corrections are due to the finite size of the basin and that is what we carefully considered. Our analysis yields satisfactory collapse plots. Strikingly, we get consistent exponents for the observational data in our theoretical analysis and more important, these effective exponents obey the theoretically derived scaling relationships. Our results are clearly consistent with a non-trivial universality class. Of course, one cannot rule out the possibility that the exponents may become trivial when the basin size becomes asymptotically large.

5.3. Scaling of Profiles and Profile Along the Mainstream

Let x be the direction parallel to the edge containing the outlets in the "substrate" plane, and y the perpendicular direction with $y = 0$ corresponding to the outlets' edge. For each sample we considered the one dimensional profiles obtained taking slices in the direction y at constant x and the corresponding roughness. The profiles and roughness averaged

over all x again show scaling properties. The height of the profile ($z(y) = \frac{1}{L}\sum_x z(x, y)$) is found to have the form:

$$z(y) = L^{\alpha} f_z\left(\frac{y}{L}\right) \tag{60}$$

with a numerical value for the exponent of $\alpha = 0.33 \pm .05$ (see Fig. 6). Likewise for the roughness $w(y) = [L^{-1}\sum_x (z(x, y) - z(y))^2]^{1/2}$ in the $y =$ const. plane

$$w(y) = L^{\alpha'} f_w\left(\frac{y}{L}\right) \tag{61}$$

with $\alpha' = 0.25 \pm 0.05$ (see Fig. 6).

In addition, we reconstructed the profile along the mainstream. This again exhibits scaling properties with a law analogous to (60) where L is replaced with the length $\mathscr{L}$ of the mainstream and with a different value of the α exponent:

$$z(l) = \mathscr{L}^{\tilde{\alpha}} \tilde{f}_z\left(\frac{l}{\mathscr{L}}\right). \tag{62}$$

In (62) l refers to the length measured along the stream. The value of $\tilde{\alpha}$ is $\tilde{\alpha} = 0.09 \pm 0.01$ definitely smaller than the value of α in (60). This is not surprising since by definition, going back up along the main stream, at each step one chooses the direction of the site with biggest area, i.e., for

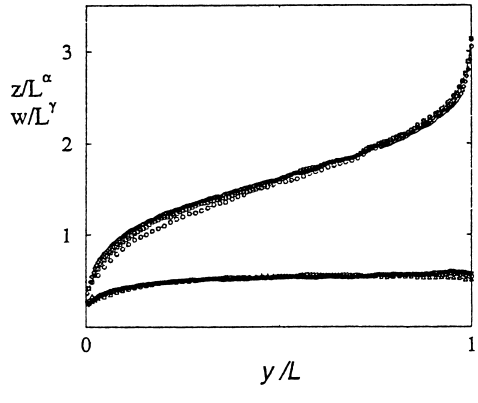

Fig. 6. Attempts to collapse the average profiles and roughness with $\alpha = 0.33$ and $\alpha' = 0.25$.

the relation (58), the direction of the smallest gradient. The resulting path is then systematically lower than a generic one.

It is very interesting to note that Eq. (62) can be recovered analytically with the correct exponent and with the explicit form of the scaling function with the following argument: the evolution along the mainstream can be regarded as an effective one dimensional problem if one takes properly into account the fluxes along the stream. Thus we argue that the behavior of $z(l, t)$ is well described by Eq. (14) replacing x on the right hand side with l^v. The value of v is expected to be given by the exponent $h^{-1} = \frac{1+H}{d_f}$ relating the area drained in a point with the upstream length relative to that point (see Eq. (52)).

Thus we are led to the following equation for the main stream evolution (after the imprinting of the drainage directions has occurred)

$$z_t(l, t) = -kl^v z_l^2(l, t) \tag{63}$$

with initial conditions

$$\begin{cases} z(l, 0) = z_0(l) \\ \partial_t z(\mathscr{L}, t) = -v. \end{cases} \tag{64}$$

This can be solved following the method described in Section 3 with the substitution $y = l^{1-\frac{v}{2}}$ unless $v = 2$. The solution is given by

$$z(l, t) = \frac{1}{\mu}\sqrt{\frac{v}{k}}\,(\mathscr{L}^\mu - l^\mu) - vt \tag{65}$$

where $\mu = 1 - \frac{v}{2}$.

Using $v = h^{-1} = \frac{1+H}{d_f}$ we get $\mu = 1 - \frac{v}{2} = 1 - \frac{1+H}{2d_f} = 0.09 \pm 0.03$, in agreement with $\tilde{d}$. The value of $k \approx 0.51$ has been extrapolated from the log–log plot of Fig. 7 (inset) where the accumulated areas along the mainstream are plotted against the upstream length. This analytical expression for z fits surprisingly well with the profiles obtained in the simulations, as is shown in Fig. 7 for the samples of size 128. Figure 8 shows the collapse of the profiles of sizes 32, 64, 128 and 256.

5.4. Bifurcation Ratios and Length Ratios

Other quantities that are used to describe the morphology of river networks are the *bifurcation ratio* R_B and the *length ratio* R_L, which can be

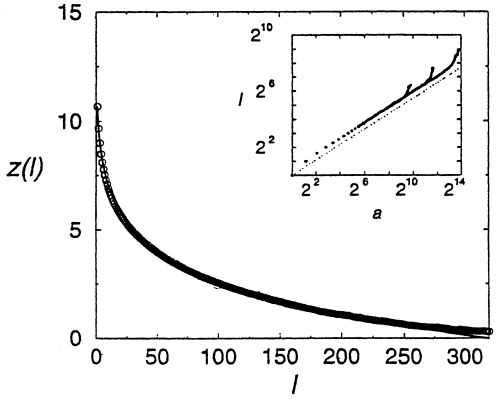

Fig. 7. Profiles along the mainstream obtained in two dimensional simulations on a 128×128 square lattice and averaged over 100 samples starting from different randomly chosen initial conditions. The solid line is the analytical result for $z + vt$ of Eq. (65) with an exponent $h = 0.55$. The value of h has been obtained from the log–log plot of the upstream lengths along the mainstream versus the corresponding areas shown in the inset. Numerical values and theoretical prediction are practically indistinguishable.

defined in the context of the Strahler's ordering scheme.[35] In the Strahler's ordering scheme, to each channel in a given network, one associates an order ω. An order 1 is assigned to streams starting in a source. Any stream emerging from an aggregation point, has the order of the biggest of the incoming streams, if they have different orders, and $\omega + 1$ if there are two (or more) incoming channels of order ω. Let N_ω and L_ω respectively denote

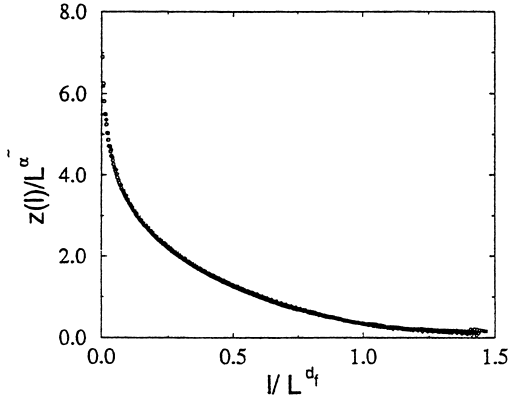

Fig. 8. Collapse of profiles along the mainstream corresponding to 32×32, 64×64, 128×128, and 256×256 square lattices obtained with $\tilde{\alpha} = 0.09$ and $\mathscr{L} \approx L^{d_f}$ with $d_f = 1.1$.

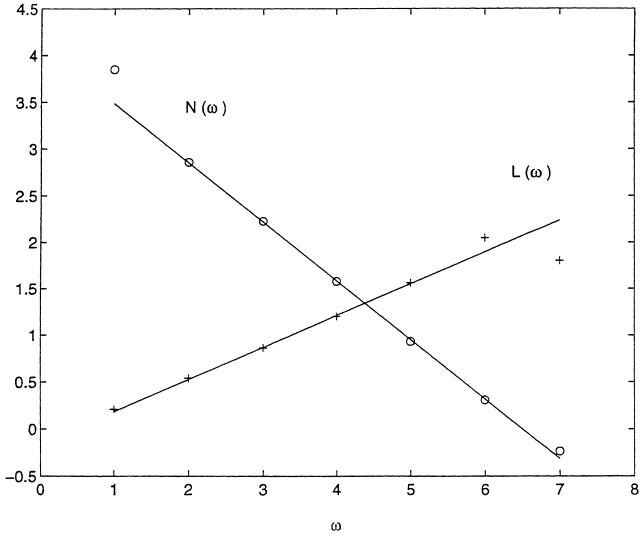

Fig. 9. Plot of $\log N(\omega)$ and $\log L(\omega)$ versus ω, averaged over 100 samples of size 128×128. The slopes are $-\log R_B$ and $\log R_L$ respectively with $R_B = 4.3 \pm 0.3$ and $R_L = 2.2 \pm 0.2$.

the number of streams of order ω and their average length. Experimentally Horton[36] found that the branching and length ratios, defined as $R_B = \frac{N_\omega}{N_{\omega+1}}$ and $R_L = \frac{L_{\omega+1}}{L_\omega}$ are essentially independent of ω in natural basins, and their value are $R_B \simeq 4$ and $R_L \simeq 2$. We tested these quantities on the networks corresponding to the stationary solutions of Eq. (4). We found that the ratios are indeed approximately independent of ω and are $R_B = 4.3 \pm 0.3$ and $R_L = 2.2 \pm 0.2$, in quite good agreement with the experimental data (Fig. 9). The fractal dimension of the network, D_f, can be readly deduced in terms of R_B, R_L and d_f. Indeed the maximum Strahler index, $\omega_{\max}$, is such that $R_L^{\omega_{\max}} \simeq L^{d_f}$, corresponding to the main stream. Thus $N_\omega \simeq R_B^{\omega_{\max}-\omega}$ and the total length of the network is $L^{D_f} \equiv \sum_\omega N_\omega L_\omega \simeq R_B^{\omega_{\max}}$, from which one obtains $D_f = d_f \ln R_B / \ln R_L = 2.0 \pm 0.2$ in accordance with expectation for a space filling structure.

6. RELATION BETWEEN THE MODEL OF LANDSCAPE EVOLUTION AND THE OPTIMAL CHANNELS NETWORK MODEL

The *Optimal Channel Network* (OCN) model has been recently proposed by Rodriguez-Iturbe *et al.*,[25, 26] and is based on a principle of minimum energy dissipation. It postulates that drainage basins, subject to energy input from precipitation, form, in their stationary state, a structure that minimizes the rate of energy dissipation.

An interesting question is whether networks resulting from the erosional dynamics are related to the optimal networks arising from the minimization of the dissipated energy. In this section we address this question, and we show that the erosion model presented in this paper, although derived in a completely independent way, is strictly related to the Optimal Channel Network model; namely, we prove that any landscape reconstructed from an optimal configuration using the slope-discharge relation is a stationary solution of the evolution equation. Superficially, this may seem to be a trivial fact because the relation between gradients and flows is verified by construction, but one should notice that the slope discharge relation alone does not implies stationarity, because the flow may not be (and in general is not) in the direction of the steepest descent in the reconstructed landscape. It is indeed a remarkable point that the minimization of the dissipated energy performs the nontrivial task of selecting networks that "come" from a consistent elevation field.

6.1. Optimal Channels Network Model

Let us briefly review the OCN model. To each landscape $\{z_i\}$ defined on a lattice as in Section 2 we associate a dissipated energy as

$$E = \sum_i k_i J_i \Delta z(i) \tag{66}$$

where $\Delta z(i)$ is the height drop along the drainage direction, J_i is the flow through the site i, and k_i is a quantity related to the soil properties such as erodability, vegetation, lithology etc. For homogeneous basins $k_i = 1$ without loss of generality.

Field investigations[37–39] show that the velocity of the flow tends to be constant throughout the network. Thus the energy dissipated to maintain the water flow, equals the potential energy associated with precipitation.[37–40] The power dissipation in a link is $J_i \Delta z_i$ and (66) represents the power expenditure in the whole system.

Using the empirical law $\Delta z(i) \sim J_i^{\gamma-1}$, with $\gamma \simeq 0.5$,[37, 40, 41] Eq. (66) can be rewritten as

$$E(T) = \sum_i J_i(T)^{\gamma}. \tag{67}$$

where $\gamma \simeq 0.5$ and T represents the oriented spanning graph associated with the landscape. The optimal channel networks consist of the configurations T which are local minima of the dissipated energy (67) in the sense specified

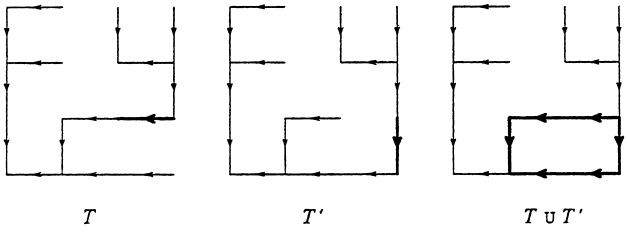

Fig. 10. Example of two *close* configurations.

below: we will say that two configurations T and T' are *close* if one can go from one to the other on just changing the direction of one link (the set of links $T \cup T'$ represent a graph with a single loop (see Fig. 10)). A configuration T is said a local minimum of the functional (67) if to each of the *close* configurations T' corresponds to a bigger energy. Note that not all changes are allowed in the sense that the new graph again needs to be loopless. Thus a local minimum is a stable configuration under a "single link flip dynamics," i.e., a dynamics in which only one link can be flipped at a given time, and is flipped only when the move does not creates loops *and* decreases the functional (67).

6.2. Connection with the Landscape Evolution Model

We will prove that any elevation field corresponding through the relation (58) to a configuration minimizing at least locally the functional (67) is a stationary solution of Eq. (4), in the sense that the landscape reconstructed from an optimal drainage network with the slope-discharge rule is consistent with the fact that the flow follows the steepest descent.

The proof is as follows: consider a configuration realizing a local minimum of the dissipated energy, and a site i. The link emerging from i will go into one of the nearest neighbors of i, let us say k. Let j be one of the other nearest neighbor such that changing the link from $i \to k$ to $i \to j$ one still gets an allowed configuration. Paths emerging from k and j will intersect downstream in a given point w (case (a)) or will never intersect until they reach their outlets (case (b)). Let S_{k_j} denote the set of all points in the path from k to w in the first case and from k to its outlet in the second (see Fig. 11). Likewise for j. Changing the link from $i \to k$ to $i \to j$ will cause only the areas of sites belonging to the sets S_{k_j} and S_{j_k} to change. In particular all areas in the set S_{j_k} will be increased by an amount equal to the area $a(i)$ contributing to the flow through i (see Eq. (41)), and all areas

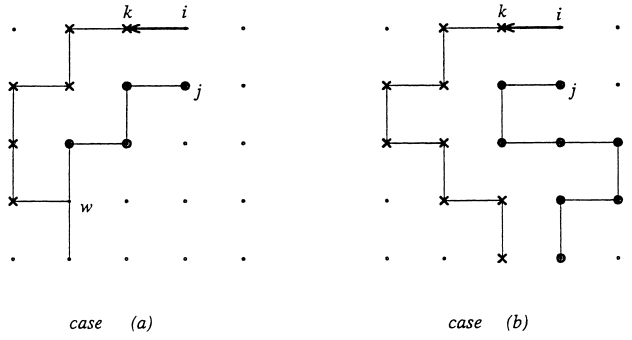

Fig. 11. Example of the two cases (a) and (b). Sites belonging to S_{k_j} are denoted with crosses, sites belonging to S_{j_k} are denoted with circles.

in the set S_{k_j} will be decreased by the same amount. Such a change will cause a change $(\Delta E)_{k \to j}$ in the dissipated energy equal to

$$(\Delta E)_{k \to j} = \sum_{x \in S_{j_k}} [(a(x)+a(i))^{\gamma} - a(x)^{\gamma}] + \sum_{x \in S_{k_j}} [(a(x)-a(i))^{\gamma} - a(x)^{\gamma}]. \quad (68)$$

where $\gamma = 1/2$ and $a(x)$ are the flows before the flip.

The condition for a configuration to be a local minimum of E translates into the set of conditions

$$(\Delta E)_{k \to j} > 0 \quad (69)$$

for each i and j such that j is a nearest neighbor of i and gives rise to a loopless configuration.

Our aim is to show that conditions (69) imply that the elevation field determined by the local minimum configuration using (58) represent a stationary solution of equation (4). To that purpose, it will be useful to express the condition of stationarity in a more explicit form. In order to be a stationary solution of Eq. (4) the elevation field determined by a graph using (58) must be such that the drainage directions derived with the steepest descent rule yields again the graph from which the elevation field originated. This would imply that if $i \to k$ is the drainage direction in the point i, the biggest drop in elevation from i to its nearest neighbors is in the direction of k. This condition reads:

$$z(j) > z(k) \quad (70)$$

for any j that is a nearest neighbor of i and different from k. In the same notation of Eqs. (68) and (69), the height at these two points can be written as:

$$\begin{aligned} z(j) &= z(w) + c \sum_{x \in S_{j_k}} a(x)^{-\frac{1}{2}} \\ z(k) &= z(w) + c \sum_{x \in S_{k_j}} a(x)^{-\frac{1}{2}} \end{aligned} \tag{71}$$

in the case (a) and

$$\begin{aligned} z(j) &= c \sum_{x \in S_{j_k}} a(x)^{-\frac{1}{2}} \\ z(k) &= c \sum_{x \in S_{k_j}} a(x)^{-\frac{1}{2}} \end{aligned} \tag{72}$$

in the case (b) (the outlets are assumed to be at zero height given that the constant drift has been subtracted). c in Eqs. (71) and (72) is a constant coming from a suitable discretization of Eq. (58). In both cases

$$z(j) - z(k) = c \left[\sum_{x \in S_{j_k}} a(x)^{-\frac{1}{2}} - \sum_{x \in S_{k_j}} a(x)^{-\frac{1}{2}} \right]. \tag{73}$$

In order to prove that Eq. (69) implies Eq. (70), let us observe that Eq. (68) can be rewritten as:

$$(\Delta E)_{k \to j} = \sum_{x \in S_{j_k}} \gamma \int_{a(x)}^{a(x)+a(i)} y^{\gamma-1} dy - \sum_{x \in S_{k_j}} \gamma \int_{a(x)-a(i)}^{a(x)} y^{\gamma-1} dy. \tag{74}$$

Because $\gamma < 1$, the first integral of Eq. (74) is smaller than $a(x)^{\gamma-1} a(i)$ and the second one is bigger than $a(x)^{\gamma-1} a(i)$. Thus Eqs. (73) and (74) imply

$$(\Delta E)_{k \to j} < \frac{\gamma}{c} a(i)(z(j) - z(k)) \tag{75}$$

where the hight $z(j)$ and $z(k)$ are evaluated before the link-flip is done. Equation (70) follows from Eqs. (69) and (75).

The proof holds in the more general case of $0 < \gamma < 1$ and Eq. (58) is substituted with $|\vec{\nabla} z| \propto J^{\gamma-1}$. The converse is not true, i.e., a stationary solution of Eq. (4) is not necessarily a local minimum of the dissipated

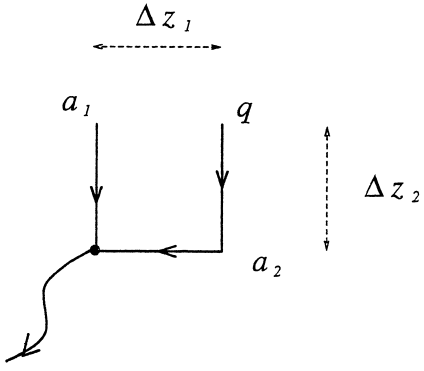

Fig. 12. One possible counterexample. A stationary solution of Eq. (4) not necessarily realizes a minimum of (67). a_1, a_2, and q represent the drained areas of the corresponding sites each independently of the others. Indeed, in the case in the figure *stationary solution* $\Rightarrow \Delta z_2 \leqslant \Delta z_1 \Rightarrow (a_2+q)^{-1/2} \leqslant a_1^{-1/2} \Leftrightarrow a_1 \leqslant a_2+q$; *not a local minimum of the energy* $\Leftarrow (a_2+q)^{1/2} + a_1^{1/2} > a_2^{1/2} + (a_1+q)^{1/2} \Leftrightarrow (a_1+q)^{1/2} - a_1^{1/2} < (a_2+q)^{1/2} - a_2^{1/2} \Leftrightarrow a_2 < a_1$.

energy (under the single link flip dynamics). Counterexamples can be easily constructed.

For example, configurations corresponding to the situation shown in Fig. 12 are stationary solutions of Eq. (4) for any $a_1 \leqslant a_2 + q$ while they are *not* local minima of (67) when $a_2 < a_1$. Thus, any choice of a_1, a_2 and q such that $a_2 < a_1 \leqslant a_2 + q$ provides a counterexample.

6.3. Time Behavior of the Topological Energy

We analyzed the behavior of the "topological" energy $E = \sum_i a(i)^{1/2}$ during the evolution of the system, performed with the algorithm described in Section 5.1. We performed several simulations starting from randomly chosen initial networks. E was always found to decrease monotonically during the dynamics. A typical behavior of the energy as a function of time, for a system of size 128×128 is shown in Fig. 13. The horizontal line represent the energy of the optimal channel network obtained using the stationary network as initial condition.

A proof of the fact that the topological energy is a decreasing function during the evolution can be given in the simple case in which the system evolves with the algorithm described in Section 5.1, where a single link is considered at each time step. In this case, the energy decreases at each step. Consider a generic network configuration and a site i, where the link emerging from i goes into the nearest neighbor k. If the elevation in another nearest neighbor, j, evaluated with the slope-area relation (58), is

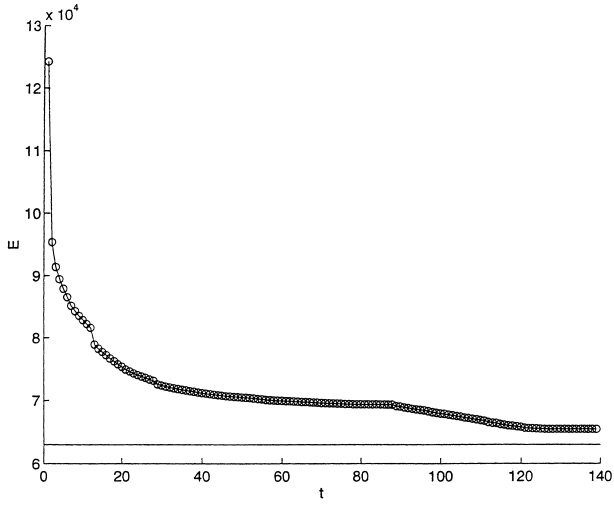

Fig. 13. Topological energy $E = \sum_i a(i)^{1/2}$ as a function of time for a 128×128 sample. The solid line below the curve is the energy of the local optimal network obtained starting with the stationary state as initial condition and using a link flip dynamic where a move is accepted only if E decreases.

smaller than the elevation in k, the link is updated: from $i \to k$ to $i \to j$. This condition corresponds to

$$z(k) - z(j) = c \left[\sum_{x \in S_{k_j}} a(x)^{-\frac{1}{2}} - \sum_{x \in S_{j_k}} a(x)^{-\frac{1}{2}} \right] > 0, \tag{76}$$

in the same notation of the preceding section. Thus, due to Eqs. (76) and (75), it follows that the spin-flip move $i \to k$ to $i \to j$ decreases the topological energy (67).

7. RESULTS IN $d = 2$ WITH ADDITIVE NOISE

7.1. Simulated Annealing

Heating the system with an additive noise term in Eq. (4), and carefully annealing, enables one to reach more stable solutions, with different statistics. Because optimal channel networks have been proved to be stationary solution of Eq. (4), and the global minimum of the dissipated energy (Eq. (67)) has been found to be characterized by mean field exponents, one might expect to approach this mean field behavior on trying to reach stable local minima on annealing of the system. This is in fact the case.

Simulations described in Section 3.2 have been repeated starting from 10 initial conditions chosen as in Section 3.2 for the equation

$$\dot{z}(t, \underline{x}) = -\alpha J(t, \underline{x}) \, |\vec{\nabla} z(t, \underline{x})|^2 + \eta(t, \underline{x}). \tag{77}$$

where $\eta(t, \underline{x})$ are independent random variables identically distributed with uniform distribution, zero mean and variance $\langle \eta(t^1, \underline{x}^1) \, \eta(t^2, \underline{x}^2) \rangle = D\delta_{t^1, t^2} \delta_{\underline{x}^1, \underline{x}^2}$.

A brief sketch of the algorithm is as follows:

(i) Generation of a random initial configuration. We generate randomly an initial configuration as described in Section 5.2.

(ii) Evolution of the configuration. The system is evolved with the algorithm described in Section 5.1 with the modification that v in Eq. (58) is replaced by $v - \eta(t, \underline{x})$, for $4 \times L \times L$ iterations ($c = -v$ in Eq. (1)).

(iii) Lowering of the variance D. In each cycle the variance D of the noise distribution is lowered by a factor $s' \simeq 0.966$ by decreasing the interval of definition of η of a factor $s = 0.983$. At the first cycle $\eta \in [-vs, vs]$, at the nth cycle $\eta \in [-vs^n, vs^n]$.

Steps (ii) and (iii) are repeated many times, until D reaches very low values ($\approx 10^{-4}$). The entire algorithm is repeated from step (i) with a new initial condition.

The distributions of drained areas and mainstream lengths show power law behavior with exponents $\tau = 1.50 \pm 0.03$ and $\psi = 1.98 \pm 0.03$, as shown in Figs. 14 and 15. The exponents for the characteristic area and length are found to be $1 + H = 1.98 \pm 0.05$ and $d_f = 1.00 \pm 0.05$ from the collapses. The exponent h has been obtained from the log–log plot of drained areas along the mainstream with respect to the corresponding upstream lengths yielding $h^{-1} = 2.00 \pm 0.05$.

The scaling of the profiles along the mainstream has also been tested. We found a logarithmic behavior of z with $\mathscr{L}$. This is in perfect agreement with the analytic argument in $d = 1$: Eq. (63) with $v = 2 - \varepsilon$ can be solved with the substitution $y = l^{1 - \frac{v}{2}}$. Taking the limit $\varepsilon \to 0$ in the solution one gets

$$z(l, t) = -\sqrt{\frac{v}{k}} \log (\mathscr{L}/l) - vt \tag{78}$$

which is the solution of Eq. (63) with $v = 2$. The comparison between the profiles obtained by simulations for a size 128 and this analytical prediction

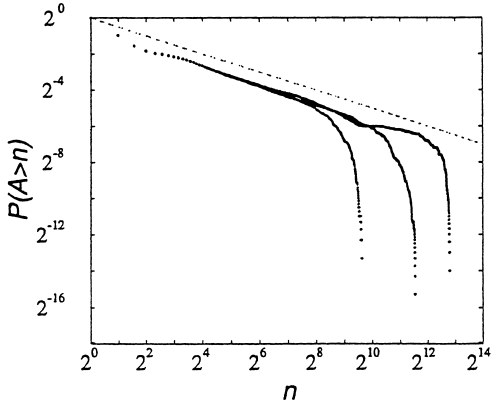

Fig. 14. Averaged distributions of drained areas for sizes 32, 64, 128. The dashed line corresponds to slope -0.5.

is shown in Fig. 16. The value of k, as in Section 5.3, has been extrapolated from the log–log plot of the areas along the mainstream versus the corresponding upstream length. Note that a naive scaling argument as in Section 3 again gives the correct result. Assuming the scaling of x, z and t with L to be

$$x \sim l \sim L, \qquad z \sim L^{\alpha}, \qquad t \sim L^{\zeta}, \tag{79}$$

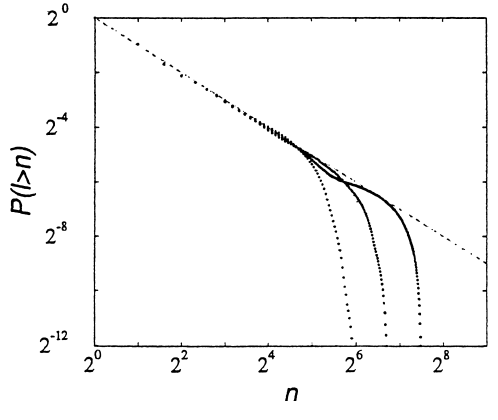

Fig. 15. Averaged distributions of upstream lengths for sizes 32, 64, 128. The dashed line corresponds to slope -1.

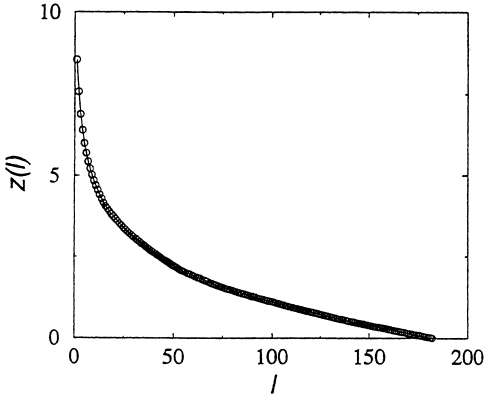

Fig. 16. Profile along the mainstream for a size 128. The solid line corresponds to the theoretical prediction.

and observing that the noise term scales as $(x^{-1}t^{-1})^{1/2} \sim L^{-\frac{1+\zeta}{2}}$, one gets

$$\begin{cases} \alpha - \zeta = 2\alpha - 1 \\ \alpha - \zeta = -\dfrac{1+\zeta}{2}. \end{cases} \tag{80}$$

This gives $\zeta = 1$ and $\alpha = 0$, in accordance with the logarithmic behavior found in (78). Also in this case, the diffusive term seems irrelevant since it should scale as $L^{\alpha-2}$.

8. MINIMUM ENERGY AND LOOPLESS STRUCTURES

8.1. Equations for the Currents

Consider a square lattice. Fix an orientation for all lattice bonds (e.g., the ones of the positive axis as in Fig. 17). On each bond b a current i_b is defined. $i_b > 0$ if it is flowing in the assigned direction, $i_b < 0$ otherwise. Uniform (unit) injection (rainfall in the case of river networks) is equivalent to the set of constraints

$$(\partial i)_x = 1 \tag{81}$$

where ∂ is a discrete version of the divergence and is a measure of the net outflow from a site (see Fig. 18):

$$(\partial i)_x = -i_1 - i_2 + i_3 + i_4 \tag{82}$$

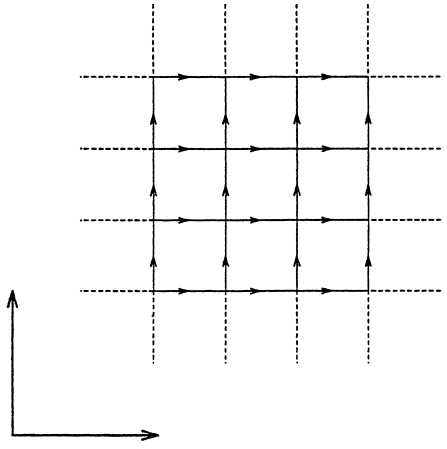

Fig. 17. Portion of a lattice showing the orientation of bonds.

We want to show that any local minimum of the cost function

$$E = \sum_b |i_b|^\gamma \tag{83}$$

when $0 < \gamma < 1$, corresponds to $i_b \neq 0$ only on the bonds of a spanning tree. In other words, we would like to prove that the networks that correspond to local minima of the dissipated energy are loopless and tree-like. The tree must be spanning due to the constraints (81): one cannot have $i_b = 0$ for all b's connected to a site so that there must be at least one outlet from each site x. Some site (or sites) must also be declared to be the global outlet. Thus loopless structures emerge as optimal solutions of Eq. (83) with the constraint (81).

Let us start with an extremely simple example: 4 sites. After implementation of (81), in the notation of Fig. 19, Eq. (83) becomes

$$E = |a|^\gamma + |a+1|^\gamma + |1-a|^\gamma + |2-a|^\gamma. \tag{84}$$

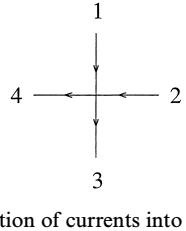

Fig. 18. Orientation of currents into and leaving a site.

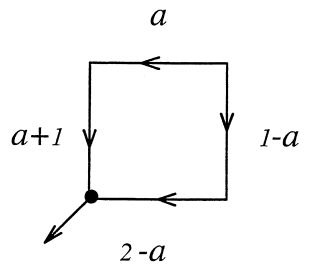

Fig. 19. Example: graph with 4 bonds. The black dot is the outlet.

In Fig. 20 one immediately sees that there are local minima in correspondence with one of the four currents being zero ($a = 2, 1, 0, -1$), corresponding to the four trees shown in Fig. 21. The explanation is simple. Suppose that $a \sim 0$ (the other cases are equivalents). Then all the terms in (84) but $|a|^\gamma$ can be expanded in Taylor series around $a = 0$. Thus, locally

$$E = 2 + 2^\gamma + |a|^\gamma + \mathcal{O}(a) \tag{85}$$

which has a cusp-like appearance because $0 < \gamma < 1$; if $\gamma < 0$ there would be a divergence instead of the cusp. Notice that $\frac{\partial E}{\partial a}|_{a=0^\pm} = \pm\infty$ and thus one cannot find the minima simply by imposing the condition $\frac{\partial E}{\partial a} = 0$. If $a \neq 0, \pm 1, 2$, $\partial^2 E/\partial a^2 < 0$ and there are no other minima of E (only maxima).

In Fig. 22, the function E versus a is plotted for various values of γ. Note that for $\gamma = 1$ all *directed* (with the currents going in the positive directions) configurations, loopless or not, have the same energy. The case $\gamma = 2$ corresponds to the resistor network case for which there is just one minimum at $a = 1/2$.

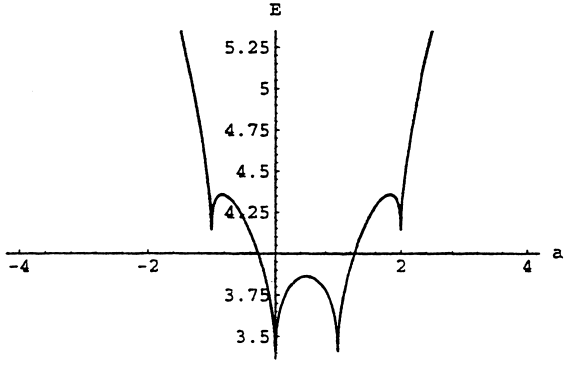

Fig. 20. Plot of the function E versus a for $\gamma = 0.5$.

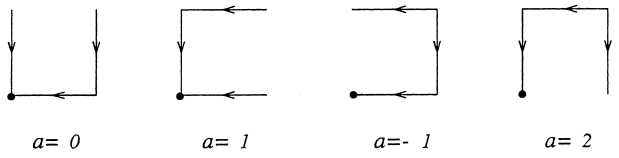

Fig. 21. Loopless configurations for the graph of Fig. 19.

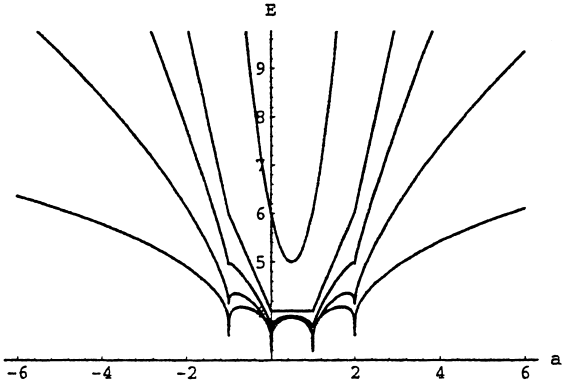

Fig. 22. Plot of the function E versus a for $\gamma = 0.25, 0.5, 0.75, 1, 2$. The lowest curve is for the smallest value of γ and the location of the curve moves up as γ increases.

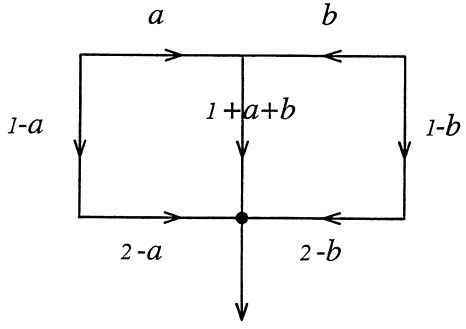

Fig. 23. Example: graph with 7 bonds. The black dot is the outlet.

Another example is that of the graph shown in Fig. 23. The energy surface is shown in Fig. 24 (to make the cusps stand out better, $-E$ has been plotted instead of E). The 15 cusps correspond to the 15 loopless configuration of this graph (see Fig. 25). Note that since there is one unknown current for each bond and one continuity equation for each site the number of independent variables is given by the number of bonds minus number of sites (excluding the outlet), which for the simple topologies we have considered is equal to the number of elementary plaquettes (this is a particular case of Euler theorem).

8.2. Lagrange Multipliers

Since we have seen that local minima occur in singular configurations, where some currents are zero, we cannot introduce the standard technique of Lagrange multipliers to find the minima of E with the constraint (81). In order to be able to do that we must regularize E as follows

$$E = \sum_b (i_b^2 + \varepsilon^2)^{\gamma/2} \tag{86}$$

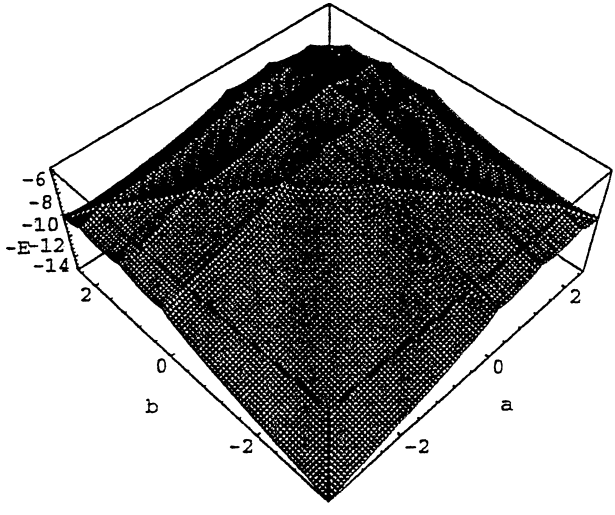

Fig. 24. Plot of the function $-E$ versus (a, b) for $\gamma = 0.5$.

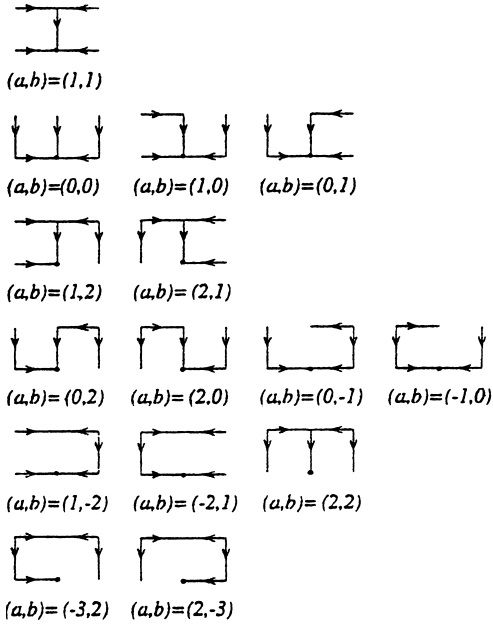

Fig. 25. The 15 loopless configurations for the graph of Fig. 23. The spanning trees with the same energy are on the same line and the lines are in the order of increasing energy. The arrows are drawn following the orientation fixed in Fig. 23.

The previous definition is recovered in the limit $\varepsilon \to 0$. If we consider again the simplest case of the 4 bonds graph, we should solve the following equations (with i_1, i_2, i_3 and i_4 as in Fig. 26).

$$0 = \frac{\partial}{\partial i_b}(E + \lambda_A(i_1 + i_2 - 1) + \lambda_B(i_3 - i_2 - 1) + \lambda_C(i_4 - i_3 - 1)), \qquad b = 1, 2, 3, 4 \tag{87}$$

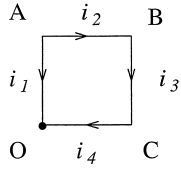

Fig. 26. Signs of the current for the example with Lagrange multipliers.

These imply (defining $\lambda_0 = 0$)

$$\begin{aligned}
&\text{(a)} \quad \lambda_0 - \lambda_A = \frac{i_1}{(i_1^2+\varepsilon^2)^{1-\gamma/2}}\,\gamma,\\
&\text{(b)} \quad \lambda_B - \lambda_A = \frac{i_2}{(i_2^2+\varepsilon^2)^{1-\gamma/2}}\,\gamma,\\
&\text{(c)} \quad \lambda_C - \lambda_B = \frac{i_3}{(i_3^2+\varepsilon^2)^{1-\gamma/2}}\,\gamma,\\
&\text{(d)} \quad \lambda_0 - \lambda_C = \frac{i_4}{(i_4^2+\varepsilon^2)^{1-\gamma/2}}\,\gamma.
\end{aligned} \tag{88}$$

If we define the r.h.s. of Eqs. (88a)–(d) as J_b with $b = 1,\ldots, 4$ respectively, then from Eq. (88) we have

$$-J_1 + J_2 + J_3 + J_4 = 0 \tag{89}$$

meaning that the *current* J_b is irrotational (i.e., $\vec{\nabla}\times\vec{J} = 0$ or equivalently $\oint d\vec{l}\cdot\vec{J} = 0$ around any loop). This, of course, has been allowed by the regularization that ensures that none of the $J_b \to \infty$, corresponding to some $i_b \to 0$. If $|i_2| \ll \varepsilon$, Eqs. (88a)–(d) have a solution

$$\begin{aligned}
i_1 &= 1 + \mathcal{O}(\varepsilon^{2-\gamma})\\
i_2 &= -\frac{\varepsilon^{2-\gamma}}{2^{1-\gamma}}\\
i_3 &= 1 + \mathcal{O}(\varepsilon^{2-\gamma})\\
i_4 &= 2 + \mathcal{O}(\varepsilon^{2-\gamma}),
\end{aligned} \tag{90}$$

and

$$-\lambda_A = \gamma, \qquad -\lambda_B = \gamma(1+2^{\gamma-1}), \qquad -\lambda_C = \gamma 2^{\gamma-1}, \tag{91}$$

and thus no divergence occurs on the r.h.s. of (88b). $-\lambda$ may then be identified as the elevation field. However the current directions do not correspond to the steepest descent.

8.3. General Proof

Given an arbitrary graph, the number l of independent loops is given by

$$\#(\text{loops}) = \#(\text{bonds}) - \#(\text{sites}) + \#(\text{connected components}) \tag{92}$$

As was observed previously, our graphs must be spanning structures, thus #(connected components) = 1. For example, in the case of an $n \times m$ rectangular lattice, $l = nm - n - m + 1$.

We want to show that any spanning tree is a local minimum of (83) and that there are no other minima.

The proof is easy if one fixes a spanning tree and properly chooses the independent variables to be the currents flowing in the bonds absent in that tree. It is immediate to see that the number of bonds absent in a tree spanning a graph is equal to the number of loops in that graph and given by Eq. (92). Consider a general structure with l independent loops. The energy

$$E = \sum_b (i_b^2 + \varepsilon^2)^{\gamma/2} \tag{93}$$

has a local minimum in all the configurations T corresponding to currents $i_b \sim \varepsilon^{2-\gamma}$ in all $b \notin T$. If we overlap T to that structure, we can assign loop currents $x_1, x_2, \ldots, x_l$ to the bonds $b \notin T$. All the others currents are determined by the constraints (81) in terms of $\vec{x}$. Thus $E = E(\vec{x})$. We will prove that $\partial E/\partial x_i = 0$ at $x_i \sim \varepsilon^{2-\gamma}$ and that the Hessian is positive definite. Indeed

$$\frac{\partial E}{\partial x_i} = \gamma \sum_b \frac{i_b}{(i_b^2 + \varepsilon^2)^{1-\gamma/2}} \frac{\partial i_b}{\partial x_i}, \tag{94}$$

where i_b is linear in x_i and $\frac{\partial i_b}{\partial x_i} = \pm 1$. Notice that in the sum (94) not all the bonds b are necessarily present. For example, in the case shown in Fig. 26 in $\partial E/\partial x_1$ at least the contributions from the bonds x_2, x_3 and x_4 are absent. This implies that only in one term of (94) $i_b \sim 0$ and it corresponds to $i_b = x_i$. All the others are finite when $\vec{x} \to 0$. Then, $\frac{\partial E}{\partial x_i} = 0$ implies

$$x_i = -\varepsilon^{2-\gamma} \sum_b{}' |i_b|^{\gamma-1} \operatorname{sgn}(i_b) \frac{\partial i_b}{\partial x_i} \simeq \varepsilon^{2-\gamma}, \qquad \varepsilon \sim 0 \tag{95}$$

and the sum $\sum'$ is over all the terms present in (94) but b: $i_b = x_i$.

$$H_{ij} = \frac{\partial^2 E}{\partial x_i \, \partial x_j} = \gamma \sum_b{}'' \frac{(\gamma-1)\, i_b^2 + \varepsilon^2}{(i_b^2+\varepsilon^2)^{2-\gamma/2}} \frac{\partial i_b}{\partial x_i} \frac{\partial i_b}{\partial x_j} \qquad i \neq j, \tag{96}$$

where in the $\sum''$ the contributions from b with $i_b = x_k$ are absent. Thus, each of the $\frac{\partial^2 E}{\partial x^i \, \partial x^j}$ is finite in the $\varepsilon \to 0$ limit. When $i = j$

$$H_{ij} = \frac{\partial^2 E}{\partial x_i \, \partial x_j} = \gamma \varepsilon^{\gamma-2} + \mathcal{O}(\varepsilon^{-\gamma}), \tag{97}$$

and thus H has the form

$$H = \gamma \varepsilon^{\gamma-2} (\mathbb{I} + \varepsilon^{2-\gamma} T), \tag{98}$$

where $T_{ii} = 0$, and $T_{ij} = \frac{1}{\gamma} H_{ij}$, $i \neq j$. This implies that the eigenvalues of H, for sufficiently low ε are all positive, confirming that (95) is indeed a minimum.

Furthermore, one can see that closing one or more loops with finite ($\mathcal{O}(\varepsilon^0)$) currents (taking one or more x_i finite) causes the appearance of one negative eigenvalue in the Hessian matrix for each added bond. If x_i is the current in this added bond, then the first derivative is $\frac{\partial E}{\partial x_i} = \gamma \, |x_i|^{\gamma-1} \operatorname{sgn}(x_b) + \gamma \sum_b' |i_b|^{\gamma-1} \frac{\partial i_b}{\partial x_i} \operatorname{sgn}(x_b)$, and the second derivative is $\frac{\partial^2 E}{\partial x_i^2} = \gamma(\gamma-1) \, |x_i|^{\gamma-2} + \sum_b' \gamma(\gamma-1) \, |i_b|^{\gamma-2} < 0$. $H_{ii} < 0$ implies that $\sum_{kj} H_{kj} z_k z_j < 0$ if $z_i \neq 0$ and $z_k = 0$, $k \neq i$. This shows that in this case the quadratic form H_{ij} is not positive definite and no local minima can be found when there are loops with non-zero currents in the $\varepsilon \to 0$ limit. This completes the proof.

When Lagrange multipliers are introduced

$$0 = \frac{\partial}{\partial i_b} \left[E + \sum_x \left[(\partial i)_x - 1 \right] \lambda_x \gamma \right] = \gamma \left[\frac{i_b}{(i_b^2+\varepsilon^2)^{1-\gamma/2}} - (d\lambda)_b \right], \tag{99}$$

where $(d\lambda)_b = \lambda_x - \lambda_y$ if b links x and y and is oriented from x to y. From Eq. (99)

$$(d\lambda)_b = \frac{i_b}{(i_b^2+\varepsilon^2)^{1-\gamma/2}}. \tag{100}$$

Corresponding to a given tree T for the i_b with $b \in T$, and because $i_b \neq 0$, we have

$$(d\lambda)_b = |i_b|^{\gamma-1} \operatorname{sgn}(i_b) + \mathcal{O}(\varepsilon^{2-\gamma}), \tag{101}$$

whereas, for $b \notin T$, Eq. (95) gives:

$$(d\lambda)_b = \frac{i_b}{(i_b^2+\varepsilon^2)^{1-\gamma/2}} = -\sum_b{}' \operatorname{sgn}(i_b) \frac{\partial i_b}{\partial x_i} |i_b|^{\gamma-1}, \tag{102}$$

where the sum has the same meaning as in (95). Notice that the neglected terms in (101) come from the x_i dependence of i_b.

Let us verify that (101) and (102) are consistent. With reference to Fig. 27, all bonds on the side (1) have a current $i_b \to i_b + x$ when $x = 0 \to x \neq 0$, whereas on the side (2) $i_b \to i_b - x$. On the side (3) the currents do not depend on x. Thus from Eq. (102) one gets

$$(d\lambda)_{b^*} = -\sum_{b \in \text{side } 1} |i_b|^{\gamma-1} \operatorname{sgn}(i_b) + \sum_{b \in \text{side } 2} |i_b|^{\gamma-1} \operatorname{sgn}(i_b). \tag{103}$$

Let us verify that along the closed circuit in Fig. 27 one has

$$\Delta\lambda \equiv \sum_{b \in \text{side } 1 \cup (-\text{side } 2) \cup b^*} (d\lambda)_b = 0. \tag{104}$$

Due to Eq. (101):

$$\Delta\lambda \equiv \sum_{b \in \text{side } 1} |i_b|^{\gamma-1} \operatorname{sgn}(i_b) - \sum_{b \in \text{side } 2} |i_b|^{\gamma-1} \operatorname{sgn}(i_b) + (d\lambda)_{b^*} \tag{105}$$

that is indeed zero due to Eq. (103).

This also shows that the terms contributing to Eq. (102) are the ones along the unique path of T joining the extremities of the bond creating the loop.

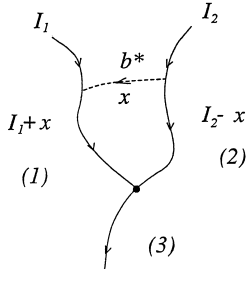

Fig. 27. Notations for the last part of the proof.

From the minimization of Eq. (83) spanning trees emerges and in correspondence of any local minima it is possible to define a scalar field λ_x satisfying Eq. (101) (proportional to the Lagrange multipliers in Eq. (99)). Eq. (101) is reminescent of the slope-discharge relation discussed in the introduction (see discussion about Eq. (5)). Thus is tempting to identify λ_x as the field of elevation.[42] However, in general, the currents defining λ_x through Eq. (101) do not follow the steepest descent route. It is the further minimization of Eq. (83) in the space of the configurations with the constraint (81) that leads to λ_x identifiable as the height field, i.e., currents consistent with steepest descent route. This follows from the theorem proved in Section 6.2.

8.4. Case $\gamma = 1$

In the case $\gamma = 1$ the previous proof does not hold. However one can prove that, all *directed* configurations, i.e., ones in which the currents flow in the positive directions correspond to the same energy, and that any other configuration has a bigger energy. One can see that in the simple example of one loop in Fig. 19.

The proof goes as follows: Let us call $V(x)$ the distance of site x from the outlet. Any site y which is a nearest neighbor of x and flowing into x has a distance $V(y) = V(x) + 1$ from the outlet. Then, since $(dV)_b = -1$,

$$\sum_x V(x) = \sum_x V(x)(\partial i)_x = -\sum_b i_b (dV)_b = \sum_b i_b , \tag{106}$$

where the $\sum_x$ is a sum over the sites and $\sum_b$ is a sum over the bonds. Note that $\sum_x V_x$ depends only on the graph topology and is *independent* of the current configuration.

If the configuration is directed, then $\sum_b i_b = \sum_b |i_b| \doteq E_d$, because all currents are positive.

In any other current configuration

$$E = \sum_b |i_b| \geqslant \left| \sum_b i_b \right| = \sum_x V_x , \tag{107}$$

and then $E \geqslant E_d$. This completes the proof.

9. CONCLUSIONS AND OUTLOOK

The model proposed and analyzed in this paper, inspite of its simplicity, captures a lot of features of landscape evolution. The evolution equation

is derived from very general considerations and provide a good qualitative and quantitative explanation for many observed facts: Hack's law, the slope-discharge relation, the power law distributions of drained areas and upstream lengths, and the bifurcation and length ratios. It also predicts the exact scaling of the average profile and the profile along the mainstream that may be deduced from observational data and would provide a good test of our theory.

A point that is still unclear is the fact that as a consequence of short freezing times corresponding to a very rapid imprinting of the landscape, the final drainage configuration of the network has a strong dependence on the initial condition. This can account for the range of values observed for τ and ψ but opens the question of what is a good physical choice for the initial configuration. Note however that this problem does not affect any of the results on the evolution of the profile and the relative scalings.

Another interesting result is that networks resulting from this erosional dynamics are related to the configurations (Optimal Channel Networks (OCN)[25,26]) arising from the minimization of the total dissipated energy. This also reveals a remarkable feature of optimal networks, in the sense that it proves that these networks originate from an elevation field——the landscapes are such that the slope-discharge relation holds at any point, and the set of drainage directions corresponds to the given network. The theorem on the occurrence of spanning networks as a consequence of the minimization of the dissipated energy justifies the conventional assumption of assigning a well defined direction for the flow. In fact, it states that in a "semicontinuum" formulation, in which the flow can split in more directions, each loopless spanning tree is a local minimum of the dissipated energy, and no other minima exist. Another interesting point is that the dissipated energy has been found indeed to monotonically decrease during the evolution.

Lastly, we believe that our results on optimal transportation networks could possibly be of interest in other problems where branched structure naturally arise from an optimization principle, for example, see refs. 43–45.

ACKNOWLEDGMENTS

This work was supported by INFM, NASA, NATO, NSF, The Petroleum Research Fund administered by the American Chemical Society and The Center for Academic Computing at Penn State.

REFERENCES

1. I. Rodriguez Iturbe and A. Rinaldo, *Fractal River Basins: Chance and Self-Organization* (Cambridge University Press, New York, 1996).

2. A. D. Howard, *Water Resour. Res.* **30**:7261 (1994).
3. R. L. Leheny and S. R. Nagel, *Phys. Rev. Lett.* **71**:1470 (1991).
4. S. Kramer and M. Marder, *Phys. Rev. Lett.* **68**:205 (1992).
5. K. Sinclair and R. C. Ball, *Phys Rev. Lett.* **76**:3360 (1996).
6. J. R. Banavar, F. Colaiori, A. Flammini, A. Giacometti, A. Maritan, and A. Rinaldo, *Phys Rev. Lett.* **78**:4522 (1997).
7. D. G. Tartobon, R. L. Bras, and I. Rodriguez-Iturbe, *Water Resour. Res.* **24**:1317 (1988).
8. D. G. Tartobon, R. L. Bras, and I. Rodriguez-Iturbe, *Water Resour. Res.* **26**:2243 (1990).
9. I. Rodriguez-Iturbe, R. L. Bras, E. Ijjasz-Vasquez, and D. G. Tarboton, *Water Resour. Res.* **28**:988 (1992).
10. D. R. Montgomery and W. E. Dietrich, *Nature* **336**:232 (1988).
11. J. T. Hack, *U. S. Geol. Surv. Prof. Paper* **294B** (1957).
12. For a recent accurate analysis of Hack's law see: R. Rigon, I. Rodriguez-Iturbe, A. Maritan, A, Giacometti, D. G. Tarboton, and A. Rinaldo, *Water Resour. Res.* **32**:3367 (1997).
13. B. B. Mandelbrot, *The Fractal Geometry of Nature* (Freeman, New York, 1983).
14. D. R. Montgomery and W. E. Dietrich, *Science* **255**:826 (1992).
15. A. Maritan, F. Toigo, J. Koplik, and J. R. Banavar, *Phys. Rev. Lett.* **69**:3193 (1992).
16. M. Marsili, A. Maritan, F. Toigo, and J. R. Banavar, *Review of Modern Physics* **68**:963 (1996).
17. A. L. Barabasi and H. E. Stanley, *Fractal Concepts in Fractal Growth* (Cambridge, Cambridge University Press, 1995).
18. E. Somfai and L. M. Sander, *Phys. Rev. E* **56**:R5 (1997).
19. R. Pastor-Satorras and D. H. Rothman, *Phys. Rev. Lett.* **80**:4349 (1998).
20. G. Caldarelli, A. Giacometti, A. Maritan, I. Rodriguez-Iturbe, and A. Rinaldo, *Phys. Rev. E* **53**:R4865, (1997). A. Giacometti, A. Maritan, and J. Banavar, *Phys. Rev. Lett.* **75**:577 (1995).
21. J. M. Burgers, *The Nonlinear Diffusion Equation* (Riedel, Boston, 1974).
22. A. Maritan, A. Rinaldo, R. Rigon, I. Rodriguez-Iturbe, and A. Giacometti, *Phys. Rev. E* **53**:1501 (1996).
23. A. Maritan, F. Colaiori, A. Flammini, M. Cieplak, and J. R. Banavar, *Science* **272**:984 (1996).
24. F. Colaiori, A. Flammini, A. Maritan, and J. R. Banavar, *Phys. Rev. E* **55**:1298 (1997).
25. I. Rodriguez-Iturbe, A. Rinaldo, R. Rigon, R. L. Bras, and E. Ijjasz-Vasquez, *Geophys. Res. Lett.* **19**:889 (1992).
26. I. Rodriguez-Iturbe, A. Rinaldo, R. Rigon, R. L. Bras, and E. Ijjasz-Vasquez, *Water Resour. Res.* **28**:1095 (1992).
27. A. Rinaldo, A. Maritan, F. Colaiori, A. Flammini, R. Rigon, I. Rodriguez-Iturbe, and J. R. Banavar, *Phys. Rev. Lett.* **76**:3364 (1996).
28. H. Takayasu, I. Nishikawa, and H. Tasaki, *Phys. Rev. A* **37**:3110 (1988).
29. H. Takayasu, M. Takayasu, A. Provata, and G. Huber, *J. Stat. Phys.* **65**:725 (1991).
30. J. S. Smaller, *Shock Waves and Reaction-Diffusion Equations* (Springer Verlag, New York, 1994).
31. A. Maritan, J. R. Banavar, M. Cieplak, F. Colaiori, A. Flammini, A. Giacometti, A. Rinaldo, and I. Rodriguez-Iturbe, in *Proc. IXX Int. Conf. on Stat. Phys.*, H. Bailin, ed. (World Scientific, Singapore, 1995).
32. W. B. Langbein, *S. Geol. Surv. Prof. Paper* **968C**:1 (1947).
33. D. M. Gray, *J. Geophys, Res.* **66**:1215 (1961).
34. J. E. Muller, *Geol. Soc. Bull.* **84**:3127 (1973).
35. A. N. Strahler, *Geol. Soc. Am. Bull.* **63**:1117 (1952).

36. R. E. Horton, *Geol. Soc. Am. Bull.* **65**:275 (1945).
37. L. B. Leopold and T. Maddock, *U. S. Geol. Surv. Prof.* **252**:56 (1953).
38. M. G. Wolman, *U. S. Geol. Surv. Prof.* **272**:56 (1955).
39. L. M. Brush, *U. S. Geol. Surv. Prof.* **282f**:1 (1961).
40. L. B. Leopold, *Am. J. Sci.* **251**:606 (1953).
41. D. G. Tartobon, R. L. Bras, and I. Rodriguez-Iturbe, Parson Lab. Rep., No. 386, Dep. Civ. Eng. MIT Massachussetes, Vol. 251, p. 1 (1989).
42. In ref. 5 minimization of Eq. (83) with the constraint (81) in their continuum version, leads the authors to the conclusion that the Lagrange multipliers have to be identified with the height field. However in their treatment no spanning structures emerged. Singular structures of this type emerge quite clearly in an approach which regularizes the problem, e.g., lattice regularization, like done here. In the approach of ref. 5 it is not possible to proceed to the further minimization in the space of these singular structures, a step which is needed in order to find current-field configuration which are consistent.
43. G. A. Ledezma, A. Bejan, and M. R. Errera, *J. Appl. Phys.* **82**:89 (1997).
44. M. W. Bern and R. L. Graham, *Sci. Am.* **260**:66 (1989).
45. A. L. Barabasi, *Phys. Rev. Lett.* **76**:3750 (1996).